

Article

# Analytical Study of the Head-On Collision Process between Hydroelastic Solitary Waves in the Presence of a Uniform Current

Muhammad Mubashir Bhatti <sup>1,2</sup> and Dong Qiang Lu <sup>1,2,\*</sup>

<sup>1</sup> Shanghai Institute of Applied Mathematics and Mechanics, Shanghai University, Yanchang Road, Shanghai 200072, China; muhammad09@shu.edu.cn

<sup>2</sup> Shanghai Key Laboratory of Mechanics in Energy Engineering, Yanchang Road, Shanghai 200072, China

\* Correspondence: dqlu@shu.edu.cn

Received: 7 January 2019; Accepted: 1 March 2019; Published: 6 March 2019



**Abstract:** The present study discusses an analytical simulation of the head-on collision between a pair of hydroelastic solitary waves propagating in the opposite directions in the presence of a uniform current. An infinite thin elastic plate is floating on the surface of water. The mathematical modeling of the thin elastic plate is based on the Euler–Bernoulli beam model. The resulting kinematic and dynamic boundary conditions are highly nonlinear, which are solved analytically with the help of a singular perturbation method. The Poincaré–Lighthill–Kuo method is applied to obtain the solution of the nonlinear partial differential equations. The resulting solutions are presented separately for the left- and right-going waves. The behavior of all the emerging parameters are presented mathematically and discussed graphically for the phase shift, maximum run-up amplitude, distortion profile, wave speed, and solitary wave profile. It is found that the presence of a current strongly affects the wavelength and wave speed of both solitary waves. A graphical comparison with pure-gravity waves is also presented as a particular case of our study.

**Keywords:** nonlinear hydroelastic waves; uniform current; thin elastic plate; solitary waves; PLK method

## 1. Introduction

The interaction between a deformable body and a moving fluid has received remarkable attention due to its numerous applications in offshore, polar engineering and industrial problems. Some applications in transportation systems can be observed in the cold region, where the ice sheet is treated as runways and roads, while air-cushion vehicles are very helpful in breaking the ice. These kinds of problems involve various mathematical challenges and present significant difficulties in the mathematical modeling of wave motion and ice deformation. Most of the previous theoretical and numerical results based on linear wave theories are not applicable to large amplitude waves. Hydroelasticity is associated with the deformation of elastic bodies due to hydrodynamics excitations, and together, these excitations are a result of body deformation. In hydroelastic problems, the elastic body and the fluid motion are coupled, which indicates that the deformation of the elastic body relies on the hydrodynamic forces and vice versa. Hydroelastic problems are difficult to analyze numerically and theoretically because, on the surface of the elastic body, hydrodynamic forces actively depend on the accelerations of the surface displacements.

In the past few years, various theoretical and numerical studies have been presented with the help of the Kirchhoff–Love plate theory to examine hydroelastic wave problems. For instance, Xia and Shen [1] analyzed the nonlinear interaction between hydroelastic solitary waves covered with ice. They used a simple perturbation method to obtain the solution for the nonlinear equations. They found

that the wavelength, shape and celerity of nonlinear solitary waves depend on the wave amplitude. The wave speed is less than the wave speed in an open water region. Milewski et al. [2] discussed hydroelastic waves in deep water using a numerical method. They used a nonlinear model for an elastic plate and particularly discussed the dynamics of unforced and forced waves. Vanden-Broeck and Părău [3] investigated the generalized form of hydroelastic periodic and solitary waves in a two-dimensional channel. They derived weakly nonlinear solutions using a perturbation scheme, and fully nonlinear solutions were obtained with the help of a numerical method. Deike et al. [4] experimentally examined the behavior of nonlinear and linear waves propagating beneath an elastic sheet in the presence of flexural waves and surface tension. By using an optical method to derive a full space–time wave field, Deike et al. [4] observed that nonlinear shift occurs due to tension in a sheet by transverse motion of the fundamental mode of an elastic plate. They further noticed that the separation between associated timescales is satisfactory at each scale of a turbulent cascade which coincides with theoretical results. Wang and Lu [5] studied nonlinear hydroelastic waves traveling under an infinite elastic plate on the surface of deep water through the homotopy analysis method.

In the studies mentioned above, less attention has been given to hydroelastic waves in the presence of a uniform current. There are different reasons, i.e., thermal, wind, and tidal effects and the rotation of the earth, why ocean currents are often produced. According to engineering applications, it is essential to determine the behavior of current when it is required to perform refraction calculations, examine the water particle acceleration and velocities for force calculations on ocean structures [6] and calculate the wave height from subsurface pressure recordings. The presence of a current influences the wave speed and affects the observed wave period and the relationship between wavelengths. Physically, when the wave travels from one region to another region in the presence of a current, not only will the wavelength and wave speed change but also, probably, current-induced refraction will occur; furthermore, the wave height will be affected. Schulkes et al. [7] analyzed hydroelastic waves in the presence of a uniform current using linear potential flow theory. Bhattacharjee and Sahoo [8] addressed the interaction of flexural gravity waves with the wave current. They also used a linear approach to discuss the physical features of a floating elastic plate under the impact of a current. Later, Bhattacharjee and Sahoo [9] examined the effect of a uniform current on flexural-gravity waves that occur due to an initial disturbance at a point. Mohanty et al. [10] explored the simultaneous effects of compressive forces and a current on time-dependent hydroelastic waves with both single- and double-layer fluids propagating through a finite and infinite depth in a two-dimensional channel. They presented the asymptotic results for the Green function and the deflection of the elastic plate using the stationary phase method. Lu and Yeung [11] examined the unsteady flexural-gravity waves that occur due to the interaction of a fixed concentrated line load with the impact of a uniform current. They observed that the flexural-gravity wave motion depends on the ratio of the current speed to the group or phase speeds.

In recent decades, various authors have investigated the collision between solitary waves using different methodologies from different geometrical aspects [12–15]. Gardner et al. [16] introduced the inverse scattering transform method to determine the exact solution of the Korteweg–de Vries (KdV) equation and discussed various engrossing characteristics of the collision between solitary waves. According to this technique, one can easily obtain the solution for overtaking solitary waves, but this technique is not suitable for determining the solution of a head-on collision process between solitary waves. When two solitary waves come close to each other, they collide and transfer their positions and energies with each other. After separating, they regain their original shapes and positions. During this entire process of interaction, both solitary waves are very stable and preserve their identities. The features of solitary waves such as striking and colliding, can only be maintained in a conservative system. Su and Mirie [17] studied the head-on collision between two solitary waves with the help of the Poincaré–Lighthill–Kuo (PLK) method. Later, Mirie and Su [18] again numerically studied the head-on collision between solitary waves and observed that after the collision of solitary waves, they recovered their original amplitudes and positions; however, a difference of less than 2% was

observed. Dai [19] investigated solitary waves at the interface of a two-layer fluid and considered a rigid bottom and surface of the channel. Mirie and Su [20] examined the head-on collision between internal solitary waves using a perturbation method. With the third-order solution, they observed that the amplitude and energy of the wave train diminish with time. Later, Mirie and Su [21] considered a similar mathematical modeling [20] with a different asymptotic expansion and derived a modified form of the KdV solution. They concluded that the collision process is inelastic, and a dispersive wave train occurs behind each emerging solitary wave. Recently, Ozden and Demiray [22] explored the work of Su and Mirie [17] with a different asymptotic assumption of the trajectory functions. The order of the trajectory functions considered by Su and Mirie [17] is  $\varepsilon$ , where  $\varepsilon$  is the perturbation parameter related to the wave amplitude. Ozden and Demiray [22] considered the order of trajectory functions to be  $\varepsilon^2$  with a similar definition for  $\varepsilon$ . Marin and Öchsner [23] discussed the initial boundary value problem for a dipolar medium using the Green–Naghdi thermoelastic theory. Some more relevant studies on the head-on collision in single and two-layer fluids can be found in Refs. [24–28].

According to the previously published results, less attention has been given to hydroelastic solitary waves, and no attempt has been made to analyze the head-on collision mechanism between hydroelastic solitary waves in the presence of a uniform current. Recently, Bhatti and Lu [29] examined the head-on collision between two hydroelastic solitary waves using the Euler–Bernoulli beam model in the presence of compression. Therefore, the present study aims to discuss the head-on collision between two hydroelastic solitary waves under uniform current and surface tension effects. We apply a singular perturbation method to obtain the analytic results for the highly nonlinear coupled partial differential equations. The PLK method is the most appropriate technique to determine the collision properties, i.e., the head-on collision, wave speed, phase shift, distortion profile, and maximum run-up amplitude. The resulting series solutions are presented up to the third-order approximation. A graphical comparison with previously published results is also presented.

## 2. Mathematical Formulation

Consider a pair of nonlinear hydroelastic solitary waves propagating in the opposite directions through a finite channel. A Cartesian coordinate is selected to formulate the mathematical model, i.e., the  $x$ -axis is proposed to lie along the horizontal direction, and the  $z$ -axis is considered to lie along the vertical direction as shown in Figure 1. A thin elastic plate is floating on the surface of water at  $z = H(x, t)$ , and the horizontal bottom is located at  $z = 0$ . Let  $U_c$  be the intensity of an underlying uniform current moving from left to right ( $U_c > 0$ ). An opposing current is defined as that moving from the right to left ( $U_c < 0$ ). The normal velocity of the governing fluid is taken as zero. The fluid is supposed to be incompressible, homogenous and inviscid, and the motion be irrotational. The velocity field in terms of potential function  $\phi(x, z, t)$  satisfies

$$\nabla^2 \phi = 0, \quad (0 < z < H). \quad (1)$$

The bottom boundary condition at  $z = 0$  is written as

$$\frac{\partial \phi}{\partial z} = 0. \quad (2)$$

The kinematic boundary condition at the water–plate interface ( $z = H(x, t)$ ) is defined as [11,29]

$$\frac{\partial H}{\partial t} + U_c \frac{\partial H}{\partial x} + \nabla \phi \cdot \nabla H = \frac{\partial \phi}{\partial z}. \quad (3)$$

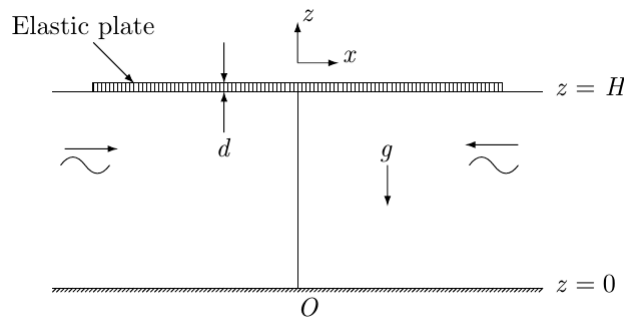


Figure 1. Schematic diagram.

The dynamic boundary condition reads [11,29]

$$\frac{\partial \phi}{\partial t} + \frac{1}{2}(U_c + |\nabla \phi|)^2 + gH - \frac{T}{\rho} \frac{\partial^2 H}{\partial x^2} + \frac{P_e}{\rho} = B_c(t). \tag{4}$$

In the above equation,  $U_c$  is a uniform current,  $g$  the gravitational acceleration,  $\rho$  the density of the fluid, and  $B_c(t)$  the Bernoulli constant which is considered to be zero.  $T$  is coefficient of surface tension of the fluid. The expression for pressure  $P_e$  consists on the Euler–Bernoulli beam theory which can be written as

$$P_e = D \frac{\partial^4 H}{\partial x^4} + M \frac{\partial^2 H}{\partial t^2}, \tag{5}$$

where  $D = Ed^3/[12(1 - \nu^2)]$  is the flexural rigidity of the plate,  $M = \rho_e d$ ,  $E$  Young’s modulus,  $d$  constant thickness,  $\nu$  Poisson’s ratio, and  $\rho_e$  the uniform mass density of the elastic plate.

With the help of Equations (1) and (2), the potential function  $\phi(x, z, t)$  can be describe using the Taylor series expansion at  $z = 0$ , we have [17]

$$\phi(x, z, t) = \sum_{i=0}^{\infty} (-1)^i \frac{z^{2i}}{(2i)!} \nabla^{2i} \Phi, \tag{6}$$

where

$$\phi(x, 0, t) = \Phi(x, t). \tag{7}$$

Using Equation (6), the kinematic and dynamic boundary condition can be obtained as

$$\frac{\partial H}{\partial t} + U_c \frac{\partial H}{\partial x} + \nabla \cdot \left[ \sum_{i=0}^{\infty} (-1)^i \frac{H^{2i+1}}{(2i+1)!} \nabla^{2i} (\nabla \Phi) \right] = 0, \tag{8}$$

$$\begin{aligned} \frac{\partial \Phi}{\partial t} + \frac{1}{2}(U_c + |\nabla \phi|)^2 + gH + \frac{P_e}{\rho} - \frac{T}{\rho} \frac{\partial^2 H}{\partial x^2} \\ + \sum_{i=1}^{\infty} (-1)^i \frac{H^{2i}}{(2i)!} \left[ \nabla^{2i} \Phi_t + U_c \nabla^{2j+1} \Phi + \frac{1}{2} \sum_{j=0}^{2i} (-1)^j C_j^{2i} \nabla^{j+1} \Phi * \nabla^{2i-j+1} \Phi \right], \end{aligned} \tag{9}$$

where

$$C_j^{2i} = \binom{2i}{j} = \frac{2i!}{j!(2i-j)!}, \tag{10}$$

is a binomial coefficient. The asterisk in Equation (9) indicates an inner vector product for the multiplication of even  $j$  and odd  $i$ .

Equations (8) and (9) can be simplified in the following form as

$$\frac{\partial H}{\partial t} + U_c \frac{\partial H}{\partial x} + \frac{\partial}{\partial x} \left[ HU + \sum_{i=1}^{\infty} (-1)^i \frac{H^{2i+1}}{(2i+1)!} \frac{\partial^{2i} U}{\partial x^{2i}} \right] = 0, \tag{11}$$

$$\begin{aligned} \frac{\partial U}{\partial t} + U_c \frac{\partial U}{\partial x} + \frac{\partial}{\partial x} \left[ gH - \frac{T}{\rho} \frac{\partial^2 H}{\partial x^2} + \frac{U^2}{2} + \frac{P_e}{\rho} + \sum_{i=1}^{\infty} (-1)^i \frac{H^{2i}}{(2i)!} \left( \frac{\partial^{2i} U}{\partial t \partial x^{2i-1}} \right. \right. \\ \left. \left. + U_c \frac{\partial^{2i} U}{\partial x^{2i}} + \frac{1}{2} \sum_{j=0}^{\infty} (-1)^j C_j^{2i} \frac{\partial^{2i-j} U}{\partial x^{2i-j}} \frac{\partial^j U}{\partial x^j} \right) \right], \end{aligned} \tag{12}$$

where  $U = \partial\Phi/\partial x$  is the tangential velocity at the bottom of the channel.

### 3. Solution Methodology

We will employ the PLK method in the ensuing section. Let us introduce the following coordinate transformations in the wave frame, we have

$$\xi_0 = \varepsilon^\delta k(x - Ct), \qquad \eta_0 = \varepsilon^\delta \bar{k}(x + \bar{C}t), \tag{13}$$

where  $k$  and  $\bar{k}$  are the wave numbers of order unity for the right- and left-going waves, respectively;  $\varepsilon$  with  $0 < \varepsilon \ll 1$  is a dimensionless parameter that represents the order of magnitude of the wave amplitude.  $C$  and  $\bar{C}$  are the wave speeds of the right- and left-going solitary waves. Using the method of strained coordinates, we introduce the following transformation of wave frame coordinates with phase functions:

$$\xi_0 = \xi - \varepsilon k \theta(\xi, \eta), \qquad \eta_0 = \eta - \varepsilon \bar{k} \varphi(\xi, \eta), \tag{14}$$

where  $\theta(\xi, \eta)$  and  $\varphi(\xi, \eta)$  are the phase functions to be deduced in the perturbation analysis. The purpose of these functions is to obtain the asymptotic approximations which acquiesce us to analyze the phase changes due to a collision.

According to Ursell’s theory of shallow water waves, we consider the scaling of the horizontal wavelength as  $\delta = 1/2$ . Although other values of  $\delta$  are also possible, i.e.,  $0, 1/4, 1/8, 1$ , these values have some restriction in our present case. However, these values are used by different authors [21,24,25] to derive various forms of the KdV equation in a two-layer fluid model but fail to give a KdV equation in our case. Later, Dai et al. [27] used  $\delta = 0$  to discuss the head-on collision among solitary waves propagating in a compressible Mooney–Rivlin elastic rod. The value of  $\delta$  plays a significant role and mainly depends upon physical and mathematical assumptions of the governing problem.

Let

$$H = H_0(1 + \zeta), \tag{15}$$

where  $\zeta$  is the non-dimensional elevation of the plate–fluid interface, and  $H_0$  is the undisturbed depth of the fluid. Considering the linear part of Equations (11) and (12), and assuming the linear solutions of  $U$  and  $\zeta$  take form of  $\exp^{i(kx - \omega t)}$ , where  $\omega$  is the wave frequency, then we have the phase speed for the right-going wave as

$$C_c = \frac{c_0}{\chi_2} \left( F + \sqrt{F^2 + \chi_1 \chi_2} \right), \tag{16}$$

and for the left-going wave it reads

$$\bar{C}_c = \frac{c_0}{\chi_2} \left( -F + \sqrt{F^2 + \chi_1 \chi_2} \right), \tag{17}$$

where

$$\chi_1 = 1 + \Gamma(kH_0)^4 + \tau(kH_0)^2 - F^2, \quad (18)$$

$$\chi_2 = 1 + \sigma(kH_0)^2, \quad (19)$$

$$c_0 = \sqrt{gH_0}, \quad \Gamma = \frac{D}{\rho g H_0^4}, \quad \sigma = \frac{M}{\rho H_0}, \quad \tau = \frac{T}{\rho g H_0^2}, \quad F = \frac{U_c}{c_0}. \quad (20)$$

The value  $c_0$  is the phase speed for pure gravity waves in shallow water of finite depth. The hydroelastic phase speed can be reduced for pure-gravity waves [17] by taking  $D \rightarrow 0$ ,  $M \rightarrow 0$ ,  $T \rightarrow 0$ , and  $U_c \rightarrow 0$ .

For convenience, let us introduce a column vector  $\mathbf{T}$  defined as

$$\mathbf{T} = \begin{pmatrix} \zeta \\ U \end{pmatrix}. \quad (21)$$

New variables are introduced in the form of the following power series:

$$\theta(\zeta, \eta) = \theta_0(\eta) + \varepsilon\theta_1(\zeta, \eta) + \varepsilon^2\theta_2(\zeta, \eta) + \dots \quad (22)$$

$$\varphi(\zeta, \eta) = \varphi_0(\zeta) + \varepsilon\varphi_1(\zeta, \eta) + \varepsilon^2\varphi_2(\zeta, \eta) + \dots \quad (23)$$

$$C = C_c \left( 1 + \varepsilon a c_1 + \varepsilon^2 a^2 c_2 + \dots \right), \quad (24)$$

$$\bar{C} = \bar{C}_c \left( 1 + \varepsilon b \bar{c}_1 + \varepsilon^2 b^2 \bar{c}_2 + \dots \right), \quad (25)$$

$$\mathbf{T} = \varepsilon \mathbf{T}_1(\zeta, \eta) + \varepsilon^2 \mathbf{T}_2(\zeta, \eta) + \varepsilon^3 \mathbf{T}_3(\zeta, \eta) + \dots, \quad (26)$$

where  $c_n$  and  $\bar{c}_n$  (i.e.,  $n = 1, 2, \dots$ ) are beneficial for removing the secular terms during the solution procedure;  $a$  and  $b$  are the amplitude factors.

#### 4. Perturbation Analysis

Substituting Equation (22) into the resulting nonlinear partial differential equations, we obtain a set of coupled differential equations with coefficients in the form of  $\varepsilon^{\frac{3}{2}}, \varepsilon^{\frac{5}{2}}, \varepsilon^{\frac{7}{2}}, \dots$ , which are expressed in a sequence as follows.

##### 4.1. Coefficients of $\varepsilon^{3/2}$

The system of first-order equations reduces to the following form as

$$k\mathbf{N} \frac{\partial \mathbf{T}_1}{\partial \zeta} + \bar{k}\bar{\mathbf{N}} \frac{\partial \mathbf{T}_1}{\partial \eta} = 0, \quad (27)$$

where

$$\mathbf{N} = \begin{pmatrix} C_c \beta_- & 1 \\ c_0^2 & C_c \beta_- \end{pmatrix}, \quad \bar{\mathbf{N}} = \begin{pmatrix} \bar{C}_c \beta_+ & 1 \\ \bar{c}_0^2 & \bar{C}_c \beta_+ \end{pmatrix}, \quad (28)$$

$$\beta_- = -1 + F\sqrt{\chi}, \quad \beta_+ = 1 + F\sqrt{\chi}, \quad \chi = \frac{c_0^2}{C_c^2}, \quad \bar{\chi} = \frac{\bar{c}_0^2}{\bar{C}_c^2}. \quad (29)$$

We define a matrix system to determine the solutions of the first order equations and higher order equations. Su and Mirie [17] introduced a new form of transformation to obtain the solutions, but the transformation fails to provide a solution for the hydroelastic wave speed (see Equation (16)). Zhu and Dai [24] successfully used a similar methodology for a two-layer fluid model, and Dai et al. [27] used a matrix system to examine the solutions for a single-layer fluid model.

The right and left characteristic vectors of  $\mathbf{N}$  and  $\bar{\mathbf{N}}$  are

$$\mathbf{R} = \begin{pmatrix} 1 \\ -C_c\beta_- \end{pmatrix}, \quad \bar{\mathbf{R}} = \begin{pmatrix} 1 \\ -\bar{C}_c\beta_+ \end{pmatrix}, \quad (30)$$

$$\mathbf{L} = \begin{pmatrix} 1, & -\frac{1}{C_c\beta_-} \end{pmatrix}, \quad \bar{\mathbf{L}} = \begin{pmatrix} 1, & -\frac{1}{\bar{C}_c\beta_+} \end{pmatrix}. \quad (31)$$

The right and left characteristic vectors in Equations (30) and (31) are introduced to determine the solution at each order. The right characteristic vectors are helpful for obtaining the solution at each order of approximation, whereas the left characteristic vectors are beneficial for solving the coupled equations at a higher order. In higher-order approximations, the resulting equations are more complex and highly coupled. It is impossible to solve the equations directly. Therefore, left characteristic vectors are beneficial for making the coupled equations into one equation at each order of approximation.

Let us consider the solution of Equation (27) in the following form

$$\mathbf{T}_1 = aA(\xi)\mathbf{R} + bB(\eta)\bar{\mathbf{R}}, \quad (32)$$

where  $A(\xi)$  and  $B(\eta)$  are arbitrary functions to be determined in the next order.

The first-order solution can be written as

$$\zeta_1 = aA(\xi) + bB(\eta), \quad (33)$$

$$U_1 = -(\bar{C}_c\beta_+bB(\eta) + C_c\beta_-aA(\xi)). \quad (34)$$

In the above equation, by taking  $F = 0$ , the present results reduce to results similar to those obtained by Bhatti and Lu [29] for hydroelastic solitary waves.

#### 4.2. Coefficients of $\varepsilon^{5/2}$

The system of second-order equations reduces to the following form as

$$\begin{aligned} \mathbf{N}k\frac{\partial\mathbf{T}_2}{\partial\xi} + aC_ck(\mathbf{E}_1A' + \mathbf{E}_2AA' + \mathbf{E}_3A''' + \mathbf{E}_4A') \\ + \bar{\mathbf{N}}\bar{k}\frac{\partial\mathbf{T}_2}{\partial\eta} + b\bar{C}_c\bar{k}(\bar{\mathbf{E}}_1B' + \bar{\mathbf{E}}_2BB' + \bar{\mathbf{E}}_3B''' + \bar{\mathbf{E}}_4B') = 0, \end{aligned} \quad (35)$$

where  $\mathbf{E}_n$  and  $\bar{\mathbf{E}}_n$  i.e., ( $n = 1, 2, 3, 4$ ) are presented in Appendix A.

Let us assume a general solution of the following form

$$\mathbf{T}_2 = X(\xi, \eta)\mathbf{R} + Y(\xi, \eta)\bar{\mathbf{R}}. \quad (36)$$

Using Equation (36) in Equation (35), and multiplying it by  $\mathbf{L}$  and  $\bar{\mathbf{L}}$ , we obtain

$$\begin{aligned} \mathbf{L}\bar{\mathbf{N}}\bar{k}\frac{\partial X}{\partial\eta} + aC_ck(\mathbf{L}\mathbf{E}_1A' + \mathbf{L}\mathbf{E}_2AA' + \mathbf{L}\mathbf{E}_3A''' + \mathbf{L}\mathbf{E}_4A') \\ + b\bar{C}_c\bar{k}(\mathbf{L}\bar{\mathbf{E}}_1B' + \mathbf{L}\bar{\mathbf{E}}_2BB' + \mathbf{L}\bar{\mathbf{E}}_3B''' + \mathbf{L}\bar{\mathbf{E}}_4B') = 0, \end{aligned} \quad (37)$$

$$\begin{aligned} &\bar{\mathbf{L}}\bar{\mathbf{N}}\bar{\mathbf{R}}k\frac{\partial Y}{\partial \xi} + aC_c k (\bar{\mathbf{L}}\mathbf{E}_1A' + \bar{\mathbf{L}}\mathbf{E}_2AA' + \bar{\mathbf{L}}\mathbf{E}_3A''' + \bar{\mathbf{L}}\mathbf{E}_4A') \\ &+ b\bar{C}_c\bar{k} (\bar{\mathbf{L}}\bar{\mathbf{E}}_1B' + \bar{\mathbf{L}}\bar{\mathbf{E}}_2BB' + \bar{\mathbf{L}}\bar{\mathbf{E}}_3B''' + \bar{\mathbf{L}}\bar{\mathbf{E}}_4B') = 0, \end{aligned} \tag{38}$$

where  $\bar{\mathbf{L}}\bar{\mathbf{N}}\bar{\mathbf{R}}$ ,  $\bar{\mathbf{L}}\bar{\mathbf{N}}\bar{\mathbf{R}}$ ,  $\mathbf{L}\mathbf{E}_n$  and  $\bar{\mathbf{L}}\bar{\mathbf{E}}_n$  ( $n = 1, 2, 3, 4$ ) represent the inner products  $\mathbf{L} \cdot \bar{\mathbf{N}} \cdot \bar{\mathbf{R}}$ ,  $\bar{\mathbf{L}} \cdot \mathbf{N} \cdot \bar{\mathbf{R}}$ ,  $\mathbf{L} \cdot \mathbf{E}_n$  and  $\bar{\mathbf{L}} \cdot \bar{\mathbf{E}}_n$ , respectively.

The above equation is further divided into three parts namely, (i) secular terms, (ii) local terms and (iii) non-local terms.

#### 4.2.1. Secular Terms

Secular terms in Equation (37) are those terms which do not depend on  $\eta$ . The other terms cannot be treated as secular terms, because if we integrate these terms with respect to  $\eta$ , then these terms become unbounded in space and time and show a secular behavior. The secular terms are

$$\mathbf{L}\mathbf{E}_1A' + \mathbf{L}\mathbf{E}_2AA' + \mathbf{L}\mathbf{E}_3A''' = 0. \tag{39}$$

Let

$$c_1 = \frac{1}{2}, \quad k^2H_0^2 = 3a, \tag{40}$$

then Equation (39) reduces to the following form

$$\gamma A''' - 3\beta_- AA' - A' = 0, \tag{41}$$

where

$$\gamma = -\frac{1}{\beta_-} (\beta_-^2 + 3a), \quad \alpha = \sigma - \chi\tau. \tag{42}$$

The solution of the above KdV equation is found as

$$A = -\frac{1}{\beta_-} \operatorname{sech}^2 \frac{\xi}{2\sqrt{\gamma}}. \tag{43}$$

Similarly,

$$\bar{\mathbf{L}}\bar{\mathbf{E}}_1B' + \bar{\mathbf{L}}\bar{\mathbf{E}}_2BB' + \bar{\mathbf{L}}\bar{\mathbf{E}}_3B''' = 0. \tag{44}$$

Let

$$\bar{c}_1 = \frac{1}{2}, \quad \bar{k}^2H_0^2 = 3b. \tag{45}$$

Then Equation (44) reduces to the following form

$$\bar{\gamma}B''' + 3\beta_+ BB' - B' = 0, \tag{46}$$

$$B = \frac{1}{\beta_+} \operatorname{sech}^2 \frac{\eta}{2\sqrt{\bar{\gamma}}}, \tag{47}$$

where

$$\bar{\gamma} = \frac{1}{\beta_+} (\beta_+^2 + 3a). \tag{48}$$

We have obtained a third-order KdV equation for the hydroelastic wave profile. A third-order KdV profile was also presented by Bhatti and Lu [29] in the absence of a uniform current, i.e.,  $F = 0$ . Furthermore, the stiffness of the plate appears in the third-order approximation.

#### 4.2.2. Non-Local Terms

The non-local terms are not secular. However, these terms are helpful for determining the phase shifts. Therefore, we will leave these terms as they are. The non-local terms appearing in Equation (37) are

$$\mathbf{LE}_4 = 0. \tag{49}$$

It follows that

$$\theta_0 = \frac{b}{\bar{k}\bar{Y}} \int_{-\infty}^{\eta} B d\eta_1, \tag{50}$$

where

$$Y = \frac{2\beta_+\beta_- - \sqrt{\chi\bar{\chi}} - S\beta_-^2}{\beta_-(2\beta_+ + S\beta_-)}, \quad S = \frac{C_c}{\bar{C}_c}. \tag{51}$$

Similarly, we have

$$\overline{\mathbf{LE}}_4 = 0. \tag{52}$$

It follows that

$$\varphi_0 = \frac{a}{\bar{k}\bar{Y}} \int_{+\infty}^{\xi} A d\xi_1, \tag{53}$$

where

$$\bar{Y} = \frac{2\beta_-\beta_+ - \sqrt{\chi\bar{\chi}} - \bar{S}\beta_+^2}{\beta_+(2\beta_- + \bar{S}\beta_+)}, \quad \bar{S} = \frac{\bar{C}_c}{C_c}. \tag{54}$$

#### 4.2.3. Local Terms

The local terms are those terms that are helpful in examining the wave speed for the left- and right-going solitary waves. The local terms appearing in Equation (37) can be written in the following form

$$\mathbf{LNR}\bar{k} \frac{\partial X}{\partial \eta} + b\bar{C}_c\bar{k} (\mathbf{LE}_1B' + \mathbf{LE}_2BB' + \mathbf{LE}_3B''' + \mathbf{LE}_4B') = 0. \tag{55}$$

Integrating the above equation with respect to  $\eta$ , we obtain the resulting equation after simplification

$$X(\xi, \eta) = C_1b^2B + \frac{C_2b^2}{2}B^2 + \frac{C_3b^2}{\bar{\gamma}} \left( B - \frac{3\beta_+}{2}B^2 \right) + C_4abAB + a^2A_1(\xi), \tag{56}$$

where  $C_n$  ( $n = 1 \dots 4$ ) are presented in Appendix B.

Similarly

$$\overline{\mathbf{LNR}}\bar{k} \frac{\partial Y}{\partial \xi} + aC_c\bar{k} (\overline{\mathbf{LE}}_1A' + \overline{\mathbf{LE}}_2AA' + \overline{\mathbf{LE}}_3A''' + \overline{\mathbf{LE}}_4A'). \tag{57}$$

Integrating the above equation with respect to  $\xi$ , we get the resulting equation after simplification

$$Y(\xi, \eta) = \bar{C}_1 a^2 A + \frac{a^2 \bar{C}_2}{2} A^2 + \frac{\bar{C}_3 a^2}{\gamma} \left( A + \frac{3\beta_-}{2} A^2 \right) + \bar{C}_4 ab AB + b^2 B_1(\eta), \quad (58)$$

where  $\bar{C}_n$  ( $n = 1 \dots 4$ ) are presented in Appendix C. The unknown arbitrary functions  $A_1(\xi)$  and  $B_1(\eta)$  will be determined in the next order.

#### 4.3. Coefficients of $\varepsilon^{7/2}$

In the third-order system, we obtain the following equation

$$\begin{aligned} \mathbf{N}k \frac{\partial \mathbf{T}_3}{\partial \xi} + aC_c k (\mathbf{F}_1 A' + \mathbf{F}_2 AA' + \mathbf{F}_3 A' A^2 + \mathbf{F}_4 (A' A_1 + AA_1')) + \mathbf{F}_5 A_1' + \mathbf{F}_6 A_1''' \\ + \mathbf{F}_7 A' + \bar{\mathbf{F}}_8 A') + \bar{\mathbf{N}}k \frac{\partial \mathbf{T}_3}{\partial \eta} + b\bar{C}_c \bar{k} (\bar{\mathbf{F}}_1 B' + \bar{\mathbf{F}}_2 BB' + \bar{\mathbf{F}}_3 B' B^2 \\ + \bar{\mathbf{F}}_4 (B' B_1 + B_1' B) + \bar{\mathbf{F}}_5 B_1' + \bar{\mathbf{F}}_6 B_1''' + \bar{\mathbf{F}}_7 B' + \mathbf{F}_8 B') = 0, \end{aligned} \quad (59)$$

where  $\mathbf{F}_n$  and  $\bar{\mathbf{F}}_n$  i.e., ( $n = 1 \dots 8$ ) are presented in Appendix A.

Let us assume a general solution of the following form

$$\mathbf{T}_3 = X_1(\xi, \eta) \mathbf{R} + Y_1(\xi, \eta) \bar{\mathbf{R}}. \quad (60)$$

Using Equation (60) in Equation (59), and multiplying it by  $\mathbf{L}$  and  $\bar{\mathbf{L}}$ , we obtain

$$\begin{aligned} \bar{\mathbf{L}} \bar{\mathbf{N}} \bar{k} \frac{\partial X_1}{\partial \eta} + aC_c k \left[ (\mathbf{L} \mathbf{F}_1 + \mathbf{L} \mathbf{F}_2 A + \mathbf{L} \mathbf{F}_3 A^2 + \mathbf{L} \mathbf{F}_7 + \mathbf{L} \bar{\mathbf{F}}_8) A' + \mathbf{L} \mathbf{F}_5 A_1' \right. \\ \left. + \mathbf{L} \mathbf{F}_6 A_1''' + \mathbf{L} \mathbf{F}_4 (A' A_1 + AA_1') \right] + b\bar{C}_c \bar{k} \left[ (\bar{\mathbf{L}} \mathbf{F}_8 + \bar{\mathbf{L}} \mathbf{F}_1 + \bar{\mathbf{L}} \mathbf{F}_7 + \bar{\mathbf{L}} \mathbf{F}_2 B \right. \\ \left. + \bar{\mathbf{L}} \mathbf{F}_3 B^2) B' + \bar{\mathbf{L}} \mathbf{F}_4 (B' B_1 + B_1' B) + \bar{\mathbf{L}} \mathbf{F}_5 B_1' + \bar{\mathbf{L}} \mathbf{F}_6 B_1''' \right] = 0, \end{aligned} \quad (61)$$

$$\begin{aligned} \bar{\mathbf{L}} \bar{\mathbf{N}} \bar{k} \frac{\partial Y_1}{\partial \xi} + aC_c k \left[ (\bar{\mathbf{L}} \mathbf{F}_1 + \bar{\mathbf{L}} \mathbf{F}_2 A + \bar{\mathbf{L}} \mathbf{F}_3 A^2 + \bar{\mathbf{L}} \mathbf{F}_7 + \bar{\mathbf{L}} \mathbf{F}_8) A' + \bar{\mathbf{L}} \mathbf{F}_5 A_1' \right. \\ \left. + \bar{\mathbf{L}} \mathbf{F}_6 A_1''' + \bar{\mathbf{L}} \mathbf{F}_4 (A' A_1 + AA_1') \right] + b\bar{C}_c \bar{k} \left[ (\bar{\mathbf{L}} \mathbf{F}_8 + \bar{\mathbf{L}} \mathbf{F}_1 + \bar{\mathbf{L}} \mathbf{F}_7 + \bar{\mathbf{L}} \mathbf{F}_2 B \right. \\ \left. + \bar{\mathbf{L}} \mathbf{F}_3 B^2) B' + \bar{\mathbf{L}} \mathbf{F}_4 (B' B_1 + B_1' B) + \bar{\mathbf{L}} \mathbf{F}_5 B_1' + \bar{\mathbf{L}} \mathbf{F}_6 B_1''' \right] = 0, \end{aligned} \quad (62)$$

where  $\bar{\mathbf{L}} \bar{\mathbf{N}} \bar{k}$ ,  $\bar{\mathbf{L}} \bar{\mathbf{N}} \bar{k}$ ,  $\mathbf{L} \mathbf{F}_n$  and  $\bar{\mathbf{L}} \bar{\mathbf{F}}_n$  ( $n = 1 \dots 8$ ) represent the inner products  $\mathbf{L} \cdot \bar{\mathbf{N}} \cdot \mathbf{R}$ ,  $\bar{\mathbf{L}} \cdot \bar{\mathbf{N}} \cdot \bar{\mathbf{R}}$ ,  $\mathbf{L} \cdot \mathbf{F}_n$  and  $\bar{\mathbf{L}} \cdot \bar{\mathbf{F}}_n$ , respectively.

The above equation is further divided into the following three parts: (i) secular terms, (ii) local terms and (iii) non-local terms.

##### 4.3.1. Secular Terms

The secular terms appearing in this order are found as

$$(\mathbf{L} \mathbf{F}_1 + \mathbf{L} \mathbf{F}_2 A + \mathbf{L} \mathbf{F}_3 A^2) A' + \mathbf{L} \mathbf{F}_4 (A' A_1 + AA_1') + \mathbf{L} \mathbf{F}_5 A_1' + \mathbf{L} \mathbf{F}_6 A_1'''. \quad (63)$$

The above equation is simplified as

$$A_1''' - A_1' - 3\beta_- (A_1 A' + A_1' A) + (-2c_2 + C_6) A' + C_7 AA' + C_8 A^2 A'. \quad (64)$$

Upon integrating the above equation we get

$$A_1'' - A_1 - 3\beta_- A_1 A + (-2c_2 + C_6) A + \frac{C_7}{2} A^2 + \frac{C_8}{3} A^3, \quad (65)$$

where  $C_6, C_7$  and  $C_8$  are presented in Appendix B.

Let

$$c_2 = \frac{C_6}{2}. \quad (66)$$

Then the solution of Equation (64) can be written as

$$A_1 = C_9A + C_{10}A^2, \quad (67)$$

where  $C_9$  and  $C_{10}$  are presented in Appendix B.

Similarly, we have

$$(\overline{\mathbf{LF}}_1 + \overline{\mathbf{LF}}_2B + \overline{\mathbf{LF}}_3B^2)B' + \overline{\mathbf{LF}}_4 (B'B_1 + B'_1B) + \overline{\mathbf{LF}}_5B'_1 + \overline{\mathbf{LF}}_6B'_1{}'''. \quad (68)$$

The above equation is simplified as

$$B_1''' - B_1' + 3\beta_+ (B_1B' + B_1'B) - (2\bar{c}_2 + \bar{C}_6) B' - \bar{C}_7AA' - \bar{C}_8B^2B'. \quad (69)$$

Upon integrating the above equation, we obtain

$$B_1'' - B_1 + 3\beta_+B_1B - (2\bar{c}_2 + \bar{C}_6)B - \frac{\bar{C}_7}{2}B^2 - \frac{\bar{C}_8}{3}B^3, \quad (70)$$

where  $\bar{C}_6, \bar{C}_7$  and  $\bar{C}_8$  are presented in Appendix C.

Let

$$\bar{c}_2 = -\frac{\bar{C}_6}{2}. \quad (71)$$

Then the solution of Equation (69) can be written as

$$B_1 = \bar{C}_9B + \bar{C}_{10}B^2, \quad (72)$$

where  $\bar{C}_9$  and  $\bar{C}_{10}$  are presented in Appendix C.

This completes the solutions for Equations (56) and (58).

#### 4.3.2. Non-Local Terms

The non-local terms appearing in this order are found as

$$\mathbf{LF}_7A' = 0. \quad (73)$$

The above equation can be written as

$$\theta_1 = \bar{\theta}_{1,0} \int_{-\infty}^{\eta} B d\eta_1 + \bar{\theta}_{1,1} \int_{-\infty}^{\eta} B^2 d\eta_1, \quad (74)$$

where

$$\bar{\theta}_{1,0} = \frac{b}{\bar{\theta}_{1,2}} \left[ C_{11} + aC_{12}A - \frac{C_{14} + aC_{15}A}{\beta_-} \right], \quad (75)$$

$$\bar{\theta}_{1,1} = \frac{b^2}{\bar{\theta}_{1,2}} \left[ C_{13} - \frac{C_{16}}{\beta_-} \right], \quad (76)$$

$$\bar{\theta}_{1,2} = -\bar{k} \left[ \frac{2\beta_+\beta_- - \sqrt{\chi\bar{\chi}} - S\beta_-^2}{\beta_-} \right], \tag{77}$$

and  $C_n$  ( $n = 11 \dots 16$ ) are presented in Appendix B.

Similarly, we have

$$\overline{\mathbf{L}\mathbf{F}_7}B' = 0. \tag{78}$$

The above equation reduces to

$$\varphi_1 = \bar{\varphi}_{1,0} \int_{+\infty}^{\zeta} A d\zeta_1 + \bar{\varphi}_{1,1} \int_{+\infty}^{\zeta} A^2 d\zeta_1, \tag{79}$$

where

$$\bar{\varphi}_{1,0} = \frac{a}{\bar{\varphi}_{1,2}} \left[ \bar{C}_{11} + b\bar{C}_{12}B - \frac{\bar{C}_{14} + b\bar{C}_{15}B}{\beta_-} \right], \tag{80}$$

$$\bar{\varphi}_{1,1} = \frac{a^2}{\bar{\varphi}_{1,2}} \left[ \bar{C}_{13} - \frac{\bar{C}_{16}}{\beta_-} \right], \tag{81}$$

$$\bar{\varphi}_{1,2} = -k \left[ \frac{2\beta_-\beta_+ - \sqrt{\chi\bar{\chi}} - \bar{S}\beta_+^2}{\beta_+} \right], \tag{82}$$

and  $\bar{C}_n$  ( $n = 11 \dots 16$ ) are presented in Appendix C.

In Equation (74), all the terms appearing are similar to the first-order phase shift and show a simple phase shift behavior except for the third term in  $\bar{\theta}_{1,0}$ . Few terms in  $\bar{\theta}_{1,0}$  depend on  $\zeta$  when  $\eta \rightarrow +\infty$ ; therefore, the wave profile is different before and after the collision process (see Figures 6 and 7) because  $\theta_1$  enters into the argument of function  $A(\zeta)$ . A similar behavior has been observed for the left-going wave.

### 4.3.3. Local Terms

The local terms are found as

$$\begin{aligned} &\overline{\mathbf{L}\mathbf{N}\mathbf{R}}\bar{k} \frac{\partial X_1}{\partial \eta} + b\bar{C}_c\bar{k} [(\mathbf{L}\mathbf{F}_8 + \mathbf{L}\bar{\mathbf{F}}_1 + \mathbf{L}\bar{\mathbf{F}}_7 + \mathbf{L}\bar{\mathbf{F}}_2B + \mathbf{L}\bar{\mathbf{F}}_3B^2)B' \\ &+ \mathbf{L}\bar{\mathbf{F}}_4(B'B_1 + B'_1B) + \mathbf{L}\bar{\mathbf{F}}_5B'_1 + \mathbf{L}\bar{\mathbf{F}}_6B''_1] + aC_c k \mathbf{L}\bar{\mathbf{F}}_8 A' = 0. \end{aligned} \tag{83}$$

Integrating the above equation, we obtain

$$X_1 = \frac{1}{C_5} (C_{17}B + C_{18}B^2 + C_{19}B^3) + a^3 A_2(\zeta), \tag{84}$$

where  $C_{17}, C_{18}$  and  $C_{19}$  are presented in Appendix B.

Similarly, we have

$$\begin{aligned} &\overline{\mathbf{L}\mathbf{N}\mathbf{R}}k \frac{\partial Y_1}{\partial \zeta} + aC_c k [(\bar{\mathbf{L}}\mathbf{F}_1 + \bar{\mathbf{L}}\mathbf{F}_2A + \bar{\mathbf{L}}\mathbf{F}_3A^2 + \bar{\mathbf{L}}\mathbf{F}_7 + \bar{\mathbf{L}}\mathbf{F}_8)A' + \bar{\mathbf{L}}\mathbf{F}_5A'_1 \\ &+ \bar{\mathbf{L}}\mathbf{F}_6A''_1 + \bar{\mathbf{L}}\mathbf{F}_4(A'A_1 + AA'_1)] + b\bar{C}_c\bar{k}\bar{\mathbf{L}}\mathbf{F}_8 = 0. \end{aligned} \tag{85}$$

Integrating the above equation, we obtain

$$Y_1 = \frac{1}{\bar{C}_5} (\bar{C}_{17}A + \bar{C}_{18}A^2 + \bar{C}_{19}A^3) + b^3 B_2(\eta), \quad (86)$$

where  $\bar{C}_{17}$ ,  $\bar{C}_{18}$  and  $\bar{C}_{19}$  are presented in Appendix C.

In the above equation,  $A_2(\xi)$  and  $B_2(\eta)$  are the undetermined functions. For further analysis, we will end our calculations here, and the solutions for  $A_2(\xi)$  and  $B_2(\eta)$  are neglected.

## 5. Analytical Results

The series solutions in the preceding section are summarized in the following form.

The interfacial elevation at the water–plate interface can be written with the help of Equations (32) and (36), and we have

$$\zeta = \varepsilon(aA + bB) + \varepsilon^2 [X(\xi, \eta) + Y(\xi, \eta)], \quad (87)$$

where  $X(\xi, \eta)$  and  $Y(\xi, \eta)$  are defined in Equations (56) and (58).

The distortion profile can be calculated with the help of Equation (87). Therefore, the functions that are products of  $B(\eta)$  and  $A(\xi)$  must be removed. For this purpose, by taking  $B(\eta) = 0$  in Equation (87), the distortion profile at the water–plate interface can be written as

$$\zeta = a\varepsilon A + \varepsilon^2 a^2 \left[ \bar{C}_1 A + \frac{\bar{C}_2}{2} A^2 + \frac{\bar{C}_3}{\gamma} \left( A + \frac{3\beta_-}{2} A^2 \right) + a^2 A_1(\xi) \right]. \quad (88)$$

The maximum run-up  $\zeta_{\max}$  during the collision process at the water–plate interface can be obtained by taking  $A = B = 1$  in Equation (87), namely

$$\zeta_{\max} \Big|_{A=B=1} = \zeta. \quad (89)$$

Following from Equations (32) and (36), the velocity at the bottom reads

$$U = -\varepsilon [\bar{C}_c \beta_+ b B + C_c \beta_- a A] - \varepsilon^2 [C_c \beta_- X(\xi, \eta) + \bar{C}_c \beta_+ Y(\xi, \eta)]. \quad (90)$$

Using Equations (40) and (65), the series solutions for the right- and left-going wave speeds are given by

$$C = C_c \left( 1 + \frac{1}{2} \varepsilon a + \frac{C_6}{2} \varepsilon^2 a^2 + O(\varepsilon^3) \right), \quad (91)$$

$$\bar{C} = \bar{C}_c \left( 1 + \frac{1}{2} \varepsilon b - \frac{\bar{C}_6}{2} \varepsilon^2 b^2 + O(\varepsilon^3) \right). \quad (92)$$

The phase shifts for the right- and left-going wave read

$$\theta = \theta_0 + \varepsilon \theta_1 + O(\varepsilon^2), \quad (93)$$

$$\varphi = \varphi_0 + \varepsilon \varphi_1 + O(\varepsilon^2), \quad (94)$$

where  $\theta_0$ ,  $\theta_1$ ,  $\varphi_0$ , and  $\varphi_1$  are given in Equations (50), (53), (74) and (79), respectively.

## 6. Graphical Analysis

This section describes the graphical behaviors of all the physical parameters involved in the governing two-dimensional hydroelastic wave problem. To determine the results in a more significant manner, Figures 2–16 depict the water–plate interface, distortion profile, wave speed, phase shift, and maximum run-up amplitude during the collision process. We consider the physical parameters, unless otherwise stated,  $E = 10^6 \text{ N m}^{-2}$ ,  $d = 0.05 \text{ m}$ ,  $F = 0.3 \text{ m s}^{-1}$ ,  $g = 9.8 \text{ m s}^{-2}$ ,  $\rho = 10^3 \text{ kg m}^{-3}$ ,  $T = 0.075 \text{ N m}^{-1}$ ,  $H_0 = 1 \text{ m}$  and  $\rho_e = 917 \text{ kg m}^{-3}$  for the graphical results. It is worth mentioning here that by taking  $\sigma = 0$ ,  $\Gamma = 0$ ,  $\tau = 0$ , and  $F = 0$  in Equations (3) and (4), the present results reduce to those obtained by Su and Mirie [17] for pure-gravity waves.

Figure 2 shows the wave profile for different values of  $\Gamma$  and  $\sigma$ . When the effects of the elastic plate are taken into account, then significantly changes in the wave profile are observed. The parameter  $\Gamma$  is directly proportional to the plate thickness  $d$  and Young's modulus  $E$ . When  $\Gamma$  and  $\sigma$  increase, the plate becomes significantly stiffer, which produces a reactive force that opposes the deformation of hydroelastic waves. Figure 3 is plotted to see the effect of the current on the solitary wave profile. We can see from this figure that when the current is moving from right to left,  $F < 0$ ; then, the wavelength, amplitude and speed of the solitary waves are affected as shown in the region  $x \in [-50, 0]$ . However, when  $F > 0$ , a similar and converse behavior is found for the second solitary waves in the region  $x \in [0, 50]$ . Figure 4 shows that an increment in the surface tension parameter  $\tau$  significantly diminishes the wave profile and that the wave profile before and after the collision process becomes narrower as the surface tension increases. Figure 5 shows a graphical comparison with previously published results presented by Su and Mirie [17]. We can observe that when  $\Gamma = 0$ ,  $\sigma = 0$ ,  $\tau = 0$ , and  $F = 0$ , our results are in excellent agreement with those of Su and Mirie [17] for pure gravity waves, which ensures the validity of the present results and the methodology used.

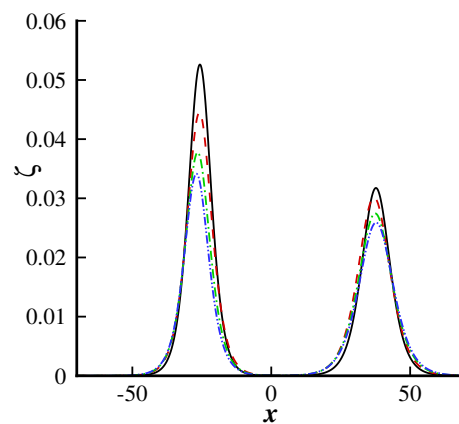


**Figure 2.** Head-on collision between two solitary waves for different values of  $\Gamma$  and  $\sigma$ . Solid line:  $\Gamma = 0$ ,  $\sigma = 0$ ; dashed line:  $\Gamma = 0.07$ ,  $\sigma = 0.5$ ; dot-dashed line:  $\Gamma = 0.09$ ,  $\sigma = 1.1$ ; dot-dot-dashed line:  $\Gamma = 0.1$ ,  $\sigma = 1.4$ .

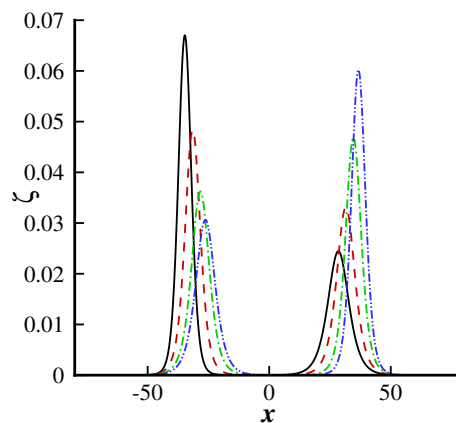


**Figure 3.** Head-on collision between two solitary waves for different values of  $F$ . Solid line:  $F = -0.3$  (opposing current); dashed line:  $F = -0.1$  (no current); dot-dashed line:  $F = 0.3$  (following current); dot-dot-dashed line:  $F = 0.5$  (following current).

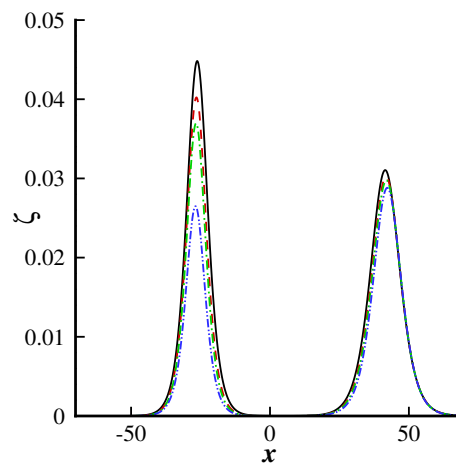


**Figure 4.** Head-on collision between two solitary waves for different values of  $\tau$ . Solid line:  $\tau = 0.5$ ; dashed line:  $\tau = 0.7$ ; dot-dashed line:  $\tau = 0.8$ ; dot-dot-dashed line:  $\tau = 1$ .

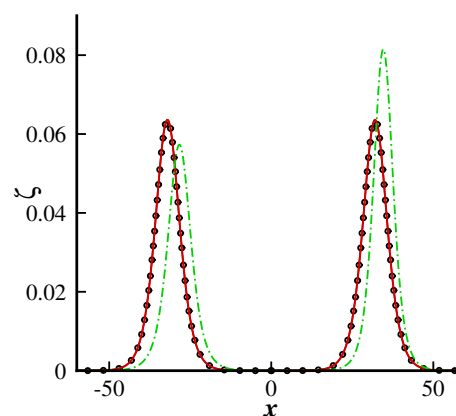


**Figure 5.** Comparison of head-on collision between two solitary waves with previously published results. Solid line (present results):  $\Gamma = 0, \sigma = 0, \tau = 0, F = 0$ ; circles (Su and Mirie [17]):  $\Gamma = 0, \sigma = 0, \tau = 0, F = 0$ ; dot-dashed line:  $\Gamma = 0.11, \sigma = 0.09, \tau = 0.01, F = 0.3$ .

Figures 6 and 7 show the distortion profile during the head-on collision process for  $F > 0$  and  $F < 0$ . In both figures, we can see that before the collision process, the wave profile is similar for  $F > 0$  and  $F < 0$ . We can observe from these figures that during the collision process, the wave profile tilts backward in the direction of wave propagation. However, the wave profile remains symmetric

before the collision process. Further, we can see that the wave profile is less affected by the following current  $F > 0$  compared with the opposing current  $F < 0$ . A similar behavior was also observed by Su and Mirie [17] for pure gravity waves and Bhatti and Lu [29] for nonlinear hydroelastic waves in the presence of a compressive force.

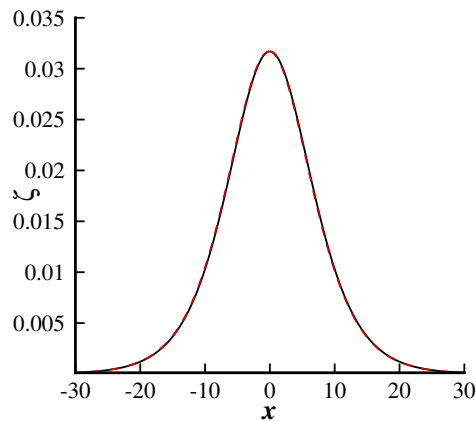


**Figure 6.** Distortion profile for  $F > 0$  (following current). Solid line: before collision; dashed line: after collision.

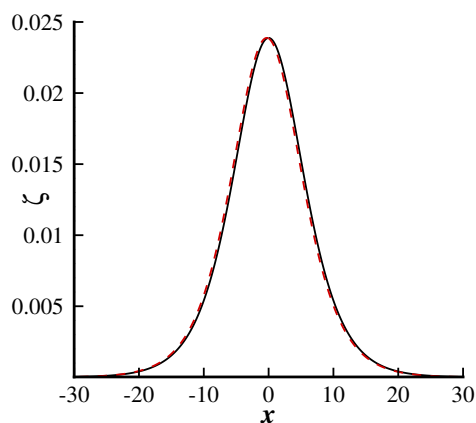


**Figure 7.** Distortion profile for  $F < 0$  (opposing current). Solid line: before collision; dashed line: after collision.

Figures 8–10 are plotted for the phase shift profile against different values of  $\Gamma$ ,  $\sigma$ ,  $\tau$  and  $F$ . It can be noted from Figure 8 that the initially phase shift profile increases due to the presence of the elastic plate, while its behavior becomes the opposite as the wave amplitude rises. Figure 9 shows that the phase shift profile increases for higher values of the following current ( $F > 0$ ), whereas its behavior is converse for higher values of the opposing current ( $F < 0$ ). Figure 10 shows the effects of the surface tension  $\tau$  on the phase shift profile. From this figure, we observe that the surface tension results are uniform throughout the domain, whereas the phase shift remarkably decreases due to a strong influence of the surface tension.

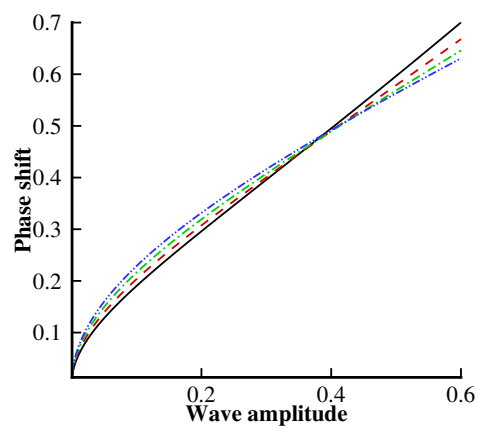


**Figure 8.** Phase shift *vs* wave amplitude. Solid line:  $\Gamma = 0, \sigma = 0$ ; dashed line:  $\Gamma = 0.11, \sigma = 0.09$ ; dot-dashed line:  $\Gamma = 0.88, \sigma = 0.18$ ; dot-dot-dashed line:  $\Gamma = 3, \sigma = 0.27$ .

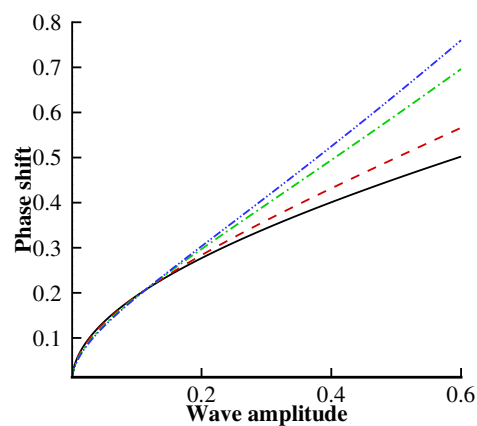


**Figure 9.** Phase shift *vs* wave amplitude. Solid line:  $F = -0.3$  (opposing current); dashed line:  $F = -0.1$  (opposing current); dot-dashed line:  $F = 0.3$  (following current); dot-dot-dashed line:  $F = 0.5$  (following current).

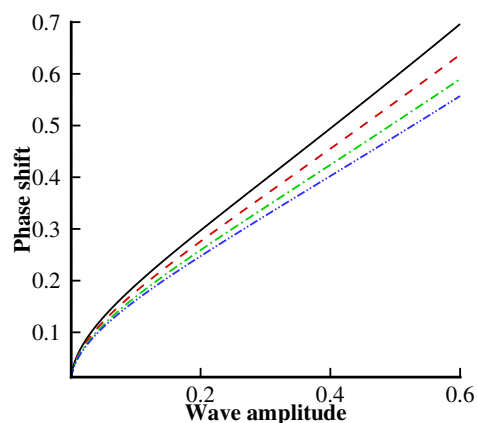


**Figure 10.** Phase shift *vs* wave amplitude. Solid line:  $\tau = 0.1$ ; dashed line:  $\tau = 0.5$ ; dot-dashed line:  $\tau = 0.8$ ; dot-dot-dashed line:  $\tau = 1$ .

Figures 11–13 show the variation of the wave speed with multiple values of  $\Gamma$ ,  $\sigma$ ,  $\tau$  and  $F$ . In Figure 11, we can observe that the wave speed decreases significantly when  $\Gamma$  increases. Furthermore, the behavior of the left-going wave speed will be opposite to that of the right-going one. Figure 12 is plotted to analyze the wave speed behavior for the left- and right-going solitary waves. In Figure 12, we can easily observe that the left-going wave speed tends to diminish with the following current  $F > 0$ , while the behavior is opposite for the right-going solitary wave. From Figure 13, we note that

the surface tension strongly influences the wave speed. We can see that the wave speed decreases due to an increment in the surface tension parameter  $\tau$ .

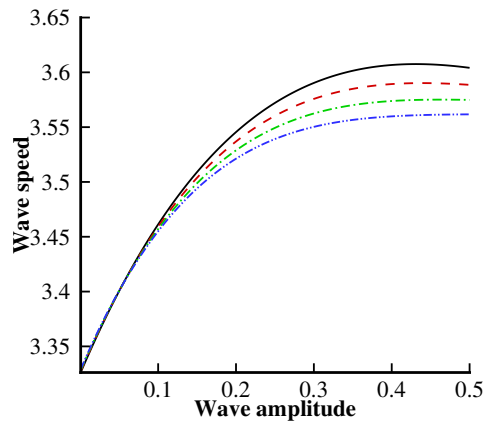


**Figure 11.** Wave speed *vs* wave amplitude. Solid line:  $\Gamma = 0.3$ ; dashed line:  $\Gamma = 0.4$ ; dot-dashed line:  $\Gamma = 0.5$ ; dot-dot-dashed line:  $\Gamma = 0.6$ .

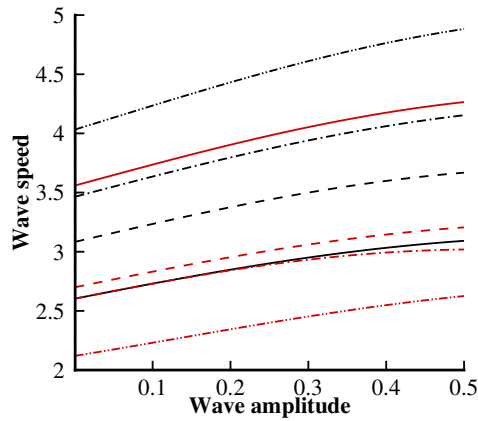


**Figure 12.** Wave speed *vs* wave amplitude. Solid line:  $F = -0.4$  (opposing current); dashed line:  $F = 0$  (no current); dot-dashed line:  $F = 0.5$  (following current); dot-dot-dashed line:  $F = 1$  (following current). Red line: left-going wave; black line: right-going wave.

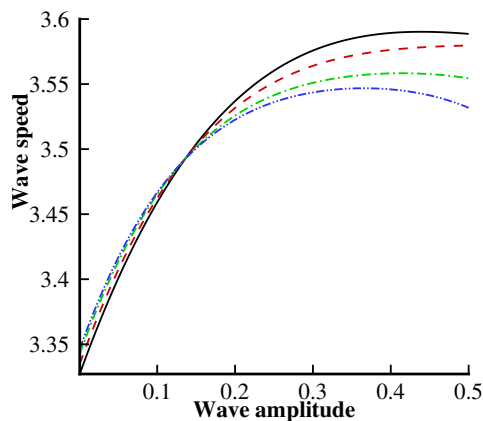


**Figure 13.** Wave speed *vs* wave amplitude. Solid line:  $\tau = 0.1$ ; dashed line:  $\tau = 0.3$ ; dot-dashed line:  $\tau = 0.5$ ; dot-dot-dashed line:  $\tau = 0.6$ .

Figures 14–16 present the variations in the maximum run-up during the collision process. It can be noted from Figure 14 that the plate deflection creates an opposing force, which tends to resist the maximum run-up amplitude. Therefore, an increment of  $\Gamma$  or  $\sigma$  tends to diminish the maximum

run-up amplitude during the collision process. However, in Figure 15, we can see that the maximum run-up amplitude increases for negative values of the current  $F < 0$ , whereas its behavior is similar for higher values of the current when  $F > 0$ . It can be observed from Figure 16 that the surface tension parameter  $\tau$  significantly affects the wave speed compared with  $\Gamma$ ,  $F$  and  $\sigma$ . An enhancement in the surface tension tends to reduce the maximum run-up amplitude.

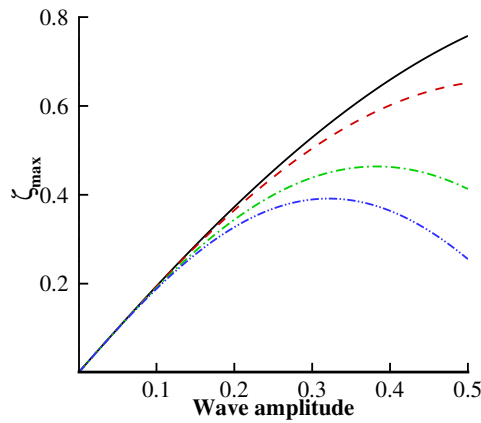


**Figure 14.** Maximum run-up *vs* wave amplitude. Solid line:  $\Gamma = \sigma = 0$ ; dashed line:  $\Gamma = 0.07, \sigma = 0.5$ ; dot-dashed line:  $\Gamma = 0.09, \sigma = 1.1$ ; dot-dot-dashed line:  $\Gamma = 0.1, \sigma = 1.4$ .

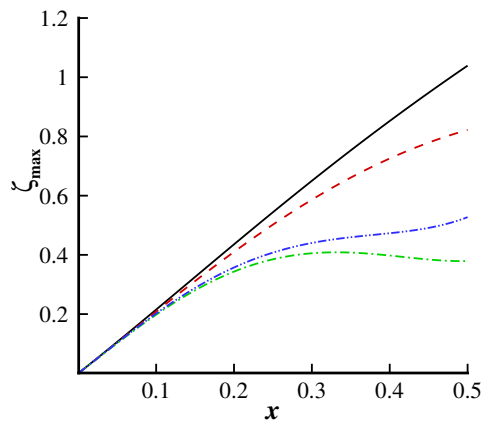


**Figure 15.** Maximum run-up *vs* wave amplitude. Solid line:  $F = -0.5$  (opposing current); dashed line:  $F = -0.4$  (opposing current); dot-dashed line:  $F = 0.4$  (following current); dot-dot-dashed line:  $F = 0.5$  (following current).

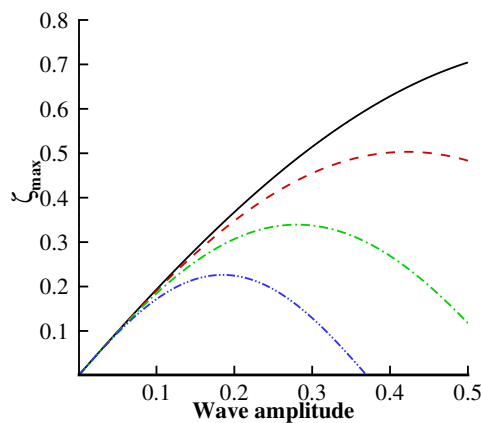


**Figure 16.** Maximum run-up *vs* wave amplitude. Solid line:  $\tau = 0.5$ ; dashed line:  $\tau = 1.0$ ; dot-dashed line:  $\tau = 1.5$ ; dot-dot-dashed line:  $\tau = 2.0$ .

## 7. Concluding Remarks

In this article, we analytically studied the behavior of a current in the head-on collision process between a pair of hydroelastic solitary waves propagating in the opposite directions. The Poincaré–Lighthill–Kuo method is successfully applied to obtain the solution for the governing nonlinear partial differential equations. The resulting solutions are presented up to the third-order approximation for right- and left-going solitary waves. The impact of different essential parameters is discussed with the help of graphs and presented mathematically for the water–plate interface, wave speed, phase shift, distortion profile, and maximum run-up amplitude during the collision process.

A graphical comparison with previously published results is also presented, and it is found that the present results are in excellent agreement, which ensures that the results for the hydroelastic wave problem are correct. It is also found that the presence of a thin elastic plate significantly reduces the amplitude of the wave profile. Furthermore, we noted that the presence of a current not only affects the wavelength and wave amplitude but also produces a remarkable effect on the wave speed. The phase shift markedly decreases due to the more significant influence of the elastic plate. It is also noted that the phase shift tends to increase for the following current, whereas its behavior is converse for the opposing current. The maximum run-up amplitude increases due to the strong influence of the following and opposing currents. It is observed that very small tilting occurs in the distortion profile during the collision process for positive values of the current, whereas greater tilting in the wave profile is seen for negative current values.

**Author Contributions:** D.Q.L.; conceptualization, M.M.B.; methodology, validation, formal analysis and writing—original draft preparation, D.Q.L.; investigation, resources, supervision, project administration, funding acquisition and writing—review and editing.

**Funding:** This research received no external funding.

**Acknowledgments:** This research was sponsored by the National Natural Science Foundation of China under Grant No. 11872239.

**Conflicts of Interest:** The authors declare that they have no conflict of interest.

## Appendix A

$$\mathbf{E}_1 = -ac_1 \begin{pmatrix} 1 \\ -C_c\beta_- \end{pmatrix}, \quad (\text{A1})$$

$$\mathbf{E}_2 = -a\beta_- \begin{pmatrix} 2 \\ -C_c\beta_- \end{pmatrix}, \quad (\text{A2})$$

$$\mathbf{E}_3 = 3a \begin{pmatrix} \frac{\beta_-}{6} \\ C_c \left( \frac{\beta_-^2}{2} + \alpha \right) \end{pmatrix}, \quad (\text{A3})$$

$$\mathbf{E}_4 = \begin{pmatrix} -abk(\bar{S}\beta_+ + \beta_-)B + 2ak\bar{k}(\bar{S}\beta_+ - \beta_-) \frac{\partial\theta_0}{\partial\eta} \\ ak\bar{C}_c \left( b\beta_+\beta_-B + \bar{k} \frac{\partial\theta_0}{\partial\eta} (\sqrt{\chi\bar{\chi}} - \beta_-\beta_+) \right) \end{pmatrix}, \quad (\text{A4})$$

$$\bar{\mathbf{E}}_1 = b\bar{c}_1 \begin{pmatrix} 1 \\ \bar{C}_c\beta_+ \end{pmatrix}, \quad (\text{A5})$$

$$\bar{\mathbf{E}}_2 = b\beta_+ \begin{pmatrix} 2 \\ \bar{C}_c\beta_+ \end{pmatrix}, \quad (\text{A6})$$

$$\bar{\mathbf{E}}_3 = 3b \begin{pmatrix} -\frac{\beta_+}{6} \\ \bar{C}_c \left( \frac{-\beta_+^2}{2} + \alpha \right) \end{pmatrix}, \quad (\text{A7})$$

$$\bar{\mathbf{E}}_4 = \begin{pmatrix} -ab\bar{k}(\beta_+ + S\beta_-)A - bk\bar{k}(\beta_+ - S\beta_-)\frac{\partial\varphi_0}{\partial\zeta} \\ b\bar{k}C_c \left( a\beta_+\beta_-A + k\frac{\partial\varphi_0}{\partial\zeta}(\sqrt{\chi\bar{\chi}} - \beta_-\beta_+) \right) \end{pmatrix}, \quad (\text{A8})$$

$$\mathbf{F}_1 = a^2 \begin{pmatrix} \frac{1}{2\gamma^2}(\bar{C}_3\bar{S}\beta_+ - \bar{C}_3\gamma + \bar{C}_1\bar{S}\beta_+\gamma - \gamma^2(\bar{C}_1 + 2c_2)) \\ C_c \left[ c_1\bar{C}_1\bar{S}\beta_+ + c_2\beta_- + \frac{9\Gamma\chi}{\gamma^2} + \frac{3\bar{C}_3\sigma}{\gamma^2} - \frac{3\bar{S}\bar{C}_3\beta_+\beta_-}{2\gamma^2} \right. \\ \left. - \frac{9\beta_-^2}{2\gamma^2} + \frac{3\bar{C}_1\sigma}{\gamma} + \frac{\bar{S}\bar{C}_3\beta_+}{2\gamma} + \frac{3\bar{S}\beta_+\beta_-\bar{C}_1}{2\gamma} - \frac{3\beta_-}{4\gamma} \right. \\ \left. - \frac{3\bar{C}_3\tau\chi}{\gamma^2} - \frac{3\bar{C}_1\tau\chi}{\gamma} \right] \end{pmatrix}, \quad (\text{A9})$$

$$\mathbf{F}_2 = a^2 \begin{pmatrix} \left[ -2 \left\{ (\bar{S}\beta_+ + \beta_-) \left( \bar{C}_1 + \frac{\bar{C}_3}{\gamma} \right) \right\} - c_1 \left( \bar{C}_2 + \frac{3\bar{C}_3\beta_-}{\gamma} \right) \right. \\ \left. + \frac{3\bar{S}\beta_+}{\gamma^2} (15\bar{C}_3\beta_- + 4\bar{C}_2\gamma + 3\bar{C}_1\gamma\beta_-) \right] \\ C_c \left[ 2\bar{S}\beta_+\beta_- \left( \bar{C}_1 + \frac{\bar{C}_3}{\gamma} \right) + 3 \left( \frac{\alpha - c_1\bar{S}\beta_+\beta_-}{\gamma^2} \right) \right. \\ \left. (15\bar{C}_3\beta_- + 4\bar{C}_2\gamma + 3\gamma\bar{C}_1\beta_-) + c_1\bar{S}\beta_+ \left( \bar{C}_2 + \frac{3\bar{C}_3\beta_-}{\gamma} \right) \right. \\ \left. + \frac{135\Gamma\beta_-}{\gamma^2} - \frac{45\beta_-^3}{8\gamma^2} + \frac{\beta_-^2}{4\gamma} \right] \end{pmatrix}, \quad (\text{A10})$$

$$\mathbf{F}_3 = a^2 \begin{pmatrix} -3c_1(\bar{S}\beta_+ + \beta_-) \left( \bar{C}_2 + \frac{3\bar{C}_3\beta_-}{\gamma} \right) + 15c_1^2\bar{S}\beta_+ \left( \frac{3\bar{C}_3\beta_-^2}{\gamma^2} + \frac{\bar{C}_2\beta_-}{\gamma} \right) \\ C_c\beta_- \left[ \frac{45c_1(3\bar{C}_3\beta_- + \bar{C}_2\gamma)(2\alpha - \bar{S}\beta_-\beta_+)}{\gamma^2} + 3c_1\bar{S}\beta_+ \right. \\ \left. \left( \bar{C}_2 + \frac{3\bar{C}_3\beta_-}{\gamma} \right) + \frac{405\chi\Gamma\beta_-}{\gamma^2} + \frac{135c_1\beta_-^3}{8\gamma^2} + \frac{27c_1\beta_-^2}{2\gamma} \right] \end{pmatrix}, \quad (\text{A11})$$

$$\mathbf{F}_4 = \mathbf{E}_2, \quad \mathbf{F}_5 = \mathbf{E}_1, \quad \mathbf{F}_6 = \mathbf{E}_3, \quad (\text{A12})$$

$$\mathbf{F}_7 = \begin{pmatrix} bC_{11}B + abC_{12}AB + b^2C_{13}B^2 + \bar{k}(\bar{S} - \beta_-) \frac{\partial \theta_1}{\partial \eta} \\ C_c \left( bC_{14}B + abC_{15}AB + b^2C_{16}B^2 + \bar{k}(\sqrt{\bar{\chi}\bar{\chi}} - \beta_- \beta_+) \frac{\partial \theta_1}{\partial \eta} \right) \end{pmatrix}, \quad (\text{A13})$$

$$\mathbf{F}_8 = -k\bar{C}_c \frac{\partial \theta_1}{\partial \xi} \begin{pmatrix} 0 \\ S^2\bar{\chi} + \beta_+^2 \end{pmatrix}, \quad (\text{A14})$$

$$\bar{\mathbf{F}}_1 = b^2 \begin{pmatrix} \frac{1}{2}C_1 + \bar{c}_2 + \frac{3C_3S\beta_-}{6\bar{\gamma}^2} + \frac{C_3}{2\bar{\gamma}} + \frac{3C_1S\beta_-}{6\bar{\gamma}} \\ \bar{C}_c \left[ -\bar{c}_2\beta_+ - \frac{1}{2}C_1S\beta_- + \frac{9\bar{\chi}\Gamma}{\bar{\gamma}^2} + \frac{3C_3\sigma}{\bar{\gamma}^2} - \frac{9\beta_+^2}{24\bar{\gamma}^2} - \frac{3C_3S\beta_- \beta_+^2}{2\bar{\gamma}} \right. \\ \left. + \frac{3c_1\sigma}{\bar{\gamma}} + \frac{3\beta_+}{4\bar{\gamma}} - \frac{C_3S\beta_-}{2\bar{\gamma}} + \frac{3c_1S\beta_- \beta_+}{2\bar{\gamma}} - 3\bar{\chi}\tau \left( \frac{C_3}{\bar{\gamma}^2} + \frac{C_1}{\bar{\gamma}} \right) \right] \end{pmatrix}, \quad (\text{A15})$$

$$\bar{\mathbf{F}}_2 = b^2 \begin{pmatrix} \left[ -2 \left\{ (\beta_+ + S\beta_-) \left( C_1 + \frac{C_3}{\bar{\gamma}} \right) \right\} + \frac{1}{2} \left( C_2 - \frac{3\bar{C}_3\beta_+}{\bar{\gamma}} \right) \right. \\ \left. + \frac{3S\beta_-}{6\bar{\gamma}^2} (15C_3\beta_+ + 4C_2\bar{\gamma} + 3C_1\bar{\gamma}\beta_+) \right] \\ \bar{C}_c \left[ 2S\beta_+\beta_- \left( C_1 + \frac{C_3}{\bar{\gamma}} \right) - 3 \left( \frac{\alpha + c_1\beta_+\beta_-}{\bar{\gamma}^2} \right) \right. \\ \left. (15\bar{C}_3\beta_- - 4\bar{C}_2\bar{\gamma} + 3\bar{\gamma}\bar{C}_1\beta_-) - \bar{c}_1S\beta_+ \left( C_2 + \frac{3C_3\beta_-}{\bar{\gamma}} \right) \right. \\ \left. - \frac{135\Gamma S^2\beta_+}{\bar{\gamma}^2} + \frac{45S^2\beta_+^3}{8\bar{\gamma}^2} + \frac{\beta_+^2}{4\bar{\gamma}} \right] \end{pmatrix}, \quad (\text{A16})$$

$$\bar{\mathbf{F}}_3 = b^2 \begin{pmatrix} -3c_1(\beta_+ + S\beta_-) \left( C_2 + \frac{3C_3\beta_-}{\bar{\gamma}} \right) + 15c_1^2S\beta_- \left( \frac{3C_3\beta_+^2}{\bar{\gamma}^2} - \frac{C_2\beta_+}{\bar{\gamma}} \right) \\ \bar{C}_c \left[ \frac{45c_1\beta_+(3C_3\beta_- - C_2\bar{\gamma})(2\alpha + S\beta_- \beta_+)}{\bar{\gamma}^2} + 3c_1S\beta_+\beta_- \right. \\ \left. \left( C_2 - \frac{3C_3\beta_+}{\bar{\gamma}} \right) + \frac{405\Gamma\bar{\chi}\beta_+^2}{\bar{\gamma}^2} - \frac{135c_1S^2\beta_+^4}{8\bar{\gamma}^2} - \frac{27c_1\beta_+^3}{\bar{\gamma}} \right] \end{pmatrix}, \quad (\text{A17})$$

$$\bar{\mathbf{F}}_4 = \bar{\mathbf{E}}_2, \quad \bar{\mathbf{F}}_5 = \bar{\mathbf{E}}_1, \quad \bar{\mathbf{F}}_6 = \bar{\mathbf{E}}_3, \quad (\text{A18})$$

$$\bar{\mathbf{F}}_7 = \begin{pmatrix} a\bar{C}_{11}A + ab\bar{C}_{12}AB + a^2\bar{C}_{13}A^2 + k(\beta_+ + S\beta_-) \frac{\partial \varphi_1}{\partial \xi} \\ \bar{C}_c \left( a\bar{C}_{14}A + ab\bar{C}_{15}AB + ab\bar{C}_{16}A^2 + k(\sqrt{\bar{\chi}\bar{\chi}} - \beta_- \beta_+) \frac{\partial \varphi_1}{\partial \xi} \right) \end{pmatrix}, \quad (\text{A19})$$

$$\bar{\mathbf{F}}_8 = \bar{k} \frac{\partial \varphi_1}{\partial \eta} \begin{pmatrix} -2\beta_- \\ C_c(\beta_-^2 - \bar{S}\sqrt{\bar{\chi}}) \end{pmatrix}, \quad (\text{A20})$$

where  $C_n$  and  $\bar{C}_n$  ( $n = 11 \dots 16$ ) are defined in Appendixs B and C.

### Appendix B

$$C_1 = -\frac{\bar{S}\beta_+ + \beta_-}{2C_5\beta_-}, \quad (\text{A21})$$

$$C_2 = \frac{\beta_+(\bar{S}\beta_+ + 2\beta_-)}{C_5\beta_-}, \quad (\text{A22})$$

$$C_3 = \frac{3\bar{S}}{C_5\beta_-} (3\beta_+^2 + 6\alpha - S\beta_-\beta_+), \quad (\text{A23})$$

$$C_4 = \frac{1}{C_5} \left( 2\beta_+ + \bar{S}\beta_- + \frac{C_c\bar{Y}(\chi - \beta_-^2)}{\beta_-} \right), \quad (\text{A24})$$

$$C_5 = 2\beta_+ - \frac{S}{\beta_-} - \frac{\sqrt{\chi}\sqrt{\bar{\chi}}}{\beta_-}, \quad (\text{A25})$$

$$C_6 = \frac{1}{2\gamma^2} (\bar{C}_3\bar{S}\beta_+ - \bar{C}_3\gamma + \bar{C}_1\bar{S}\beta_+\gamma - \gamma^2\bar{C}_1) - 2\beta_-A_2 - \frac{1}{\beta_-} \left[ c_1\bar{C}_1\bar{S}\beta_+ + c_2\beta_- + \frac{9\Gamma\chi}{\gamma^2} \right. \\ \left. + \frac{3\bar{C}_3\sigma}{\gamma^2} - \frac{3\bar{S}\bar{C}_3\beta_+\beta_-}{2\gamma^2} - \frac{9\beta_-^2}{2\gamma^2} + \frac{3\bar{C}_1\sigma}{\gamma} + \frac{\bar{S}\bar{C}_3\beta_+}{2\gamma} + \frac{3\bar{S}\beta_+\beta_-\bar{C}_1}{2\gamma} - \frac{3\beta_-}{4\gamma} - \frac{3\bar{C}_3\tau\chi}{\gamma^2} \right. \\ \left. - \frac{3\bar{C}_1\tau\chi}{\gamma} \right], \quad (\text{A26})$$

$$C_7 = \left[ -2 \left\{ (\bar{S}\beta_+ + \beta_-) \left( \bar{C}_1 + \frac{\bar{C}_3}{\gamma} \right) \right\} - c_1 \left( \bar{C}_2 + \frac{3\bar{C}_3\beta_-}{\gamma} \right) + (15\bar{C}_3\beta_- + 4\bar{C}_2\gamma \right. \\ \left. + 3\bar{C}_1\gamma\beta_-) \frac{3\bar{S}\beta_+}{\gamma^2} \right] - \frac{1}{\beta_-} \left[ 2\bar{S}\beta_+\beta_- \left( \bar{C}_1 + \frac{\bar{C}_3}{\gamma} \right) + 3 \left( \frac{\alpha - c_1\bar{S}\beta_+\beta_-}{\gamma^2} \right) (15\bar{C}_3\beta_- \right. \\ \left. + 4\bar{C}_2\gamma + 3\gamma\bar{C}_1\beta_-) + c_1\bar{S}\beta_+ \left( \bar{C}_2 + \frac{3\bar{C}_3\beta_-}{\gamma} \right) + \frac{135\Gamma\beta_-}{\gamma^2} - \frac{45\beta_-^3}{8\gamma^2} + \frac{\beta_-^2}{4\gamma} \right], \quad (\text{A27})$$

$$C_8 = -3c_1(\bar{S}\beta_+ + \beta_-) \left( \bar{C}_2 + \frac{3\bar{C}_3\beta_-}{\gamma} \right) + 15c_1^2\bar{S}\beta_+ \left( \frac{3\bar{C}_3\beta_-^2}{\gamma^2} + \frac{\bar{C}_2\beta_-}{\gamma} \right) \\ - \left[ \frac{45c_1(3\bar{C}_3\beta_- + \bar{C}_2\gamma)(2\alpha - \bar{S}\beta_-\beta_+)}{\gamma^2} + 3c_1\bar{S}\beta_+ \left( \bar{C}_2 + \frac{3\bar{C}_3\beta_-}{\gamma} \right) + \frac{405\chi\Gamma\beta_-}{\gamma^2} \right. \\ \left. + \frac{135c_1\beta_-^3}{8\gamma^2} + \frac{27c_1\beta_-^2}{2\gamma} \right], \quad (\text{A28})$$

$$C_9 = -\frac{4C_8 + 3C_7\beta_-}{9\beta_-^2}, \quad (\text{A29})$$

$$C_{10} = \frac{2C_8}{3\beta_-}. \tag{A30}$$

$$C_{11} = -c_1a(C_4 + \bar{C}_4) - (b\beta_- + 2a\bar{S}\beta_+) \left( \bar{C}_1 + \frac{\bar{C}_3}{\gamma} \right) - 3c_1(b+a) \left( \frac{\bar{C}_4\bar{S}\beta_+}{\bar{\gamma}} + \frac{C_4\beta_-}{\bar{\gamma}} \right) + c_1a\bar{S}Y + \frac{c_1a\beta_-Y}{\gamma} - \frac{c_1b\bar{S}\beta_+\bar{Y}}{\bar{\gamma}} + \frac{c_1a\beta_-}{\bar{\gamma}} + \frac{b\bar{S}\beta_+\bar{Y}}{\bar{\gamma}} + \frac{b\beta_-Y}{\bar{\gamma}} + \frac{a\beta_-Y}{\gamma}, \tag{A31}$$

$$C_{12} = -2(C_4 + \bar{C}_4)\beta_- - 2(\bar{C}_4\bar{S}\beta_+ + C_4\beta_-) + \frac{3c_1\bar{S}C_4\beta_-\beta_+}{\gamma} + \frac{3c_1C_4\beta_-^2}{\gamma} - 2\bar{S}\beta_+ \left( \bar{C}_2 + \frac{3\bar{C}_3\beta_-}{\gamma} \right) - 2\beta_-Y + \frac{9c_1\beta_-^2Y}{\gamma}, \tag{A32}$$

$$C_{13} = -2(C_4 + \bar{C}_4)\bar{S}\beta_+ - 2(\bar{C}_4\bar{S}\beta_+ + C_4\beta_-) + \frac{9c_1\bar{S}C_4\beta_+^2}{\bar{\gamma}} + \frac{9c_1C_4\beta_-\beta_+}{\bar{\gamma}} - \frac{3\bar{S}\beta_+\bar{Y}}{\bar{\gamma}} - 2\beta_- \left( \bar{C}_2 - \frac{3\bar{C}_3\beta_+}{\bar{\gamma}} \right) + 2(C_4 + \bar{C}_4)\bar{S}Y\beta_+ - 2Y(\bar{S}\beta_+ + \beta_- + \bar{C}_4\bar{S}\beta_+ + C_4\beta_-) - \frac{3c_1\beta_+\beta_-\bar{Y}}{\bar{\gamma}}, \tag{A33}$$

$$C_{14} = c_1a(\bar{C}_4\bar{S}\beta_+ + C_4\beta_-) + (b\beta_-^2 + a\beta_+^2\bar{S}^2) \left( C_1 + \frac{C_3}{\gamma} \right) + \sigma(3\bar{S}^2b - 6b\bar{S} + 3a) \left( \frac{C_4}{\gamma} + \frac{\bar{C}_4}{\gamma} \right) + \frac{3b\beta_-}{2\bar{\gamma}}(\bar{S}C_4 + C_4) + \frac{3b\bar{S}\beta_+}{2\bar{\gamma}}(\bar{S}C_4 + C_4) + \frac{3a\beta_-}{2\gamma}(\bar{S}C_4 + C_4) - a\bar{S}^2Y\beta_+\beta_- \left( \bar{C}_1 + \frac{\bar{C}_3}{\gamma} \right) + \frac{3a\beta_-^2Y}{\gamma} + \frac{3a\beta_-\beta_+\bar{S}Y}{2\gamma} + \frac{3b\beta_+^2\bar{S}Y}{2\bar{\gamma}} + \frac{3b\beta_+\beta_-\bar{S}Y}{\bar{\gamma}} + \frac{3b\beta_+\beta_-\bar{S}Y}{2\bar{\gamma}} + \frac{3a\beta_+\beta_-\bar{S}Y}{2\bar{\gamma}} - \frac{4b\beta_+\bar{S}^2\bar{Y}}{\bar{\gamma}} + \frac{4a\beta_-\bar{S}Y}{\gamma} - \frac{7b\bar{S}\beta_+\bar{Y}}{2\bar{\gamma}} + \frac{3b\bar{S}\beta_+\beta_-}{2\bar{\gamma}} - \frac{3a\bar{S}\beta_+\beta_-}{2\bar{\gamma}} - 3ab\chi\tau \left( \frac{b}{\bar{\gamma}} + \frac{a}{\gamma} \right) (C_4 + \bar{C}_4) - c_1a\bar{S}\beta_-\bar{Y} + a\bar{S}\sqrt{\chi\bar{\chi}}Y \left( \bar{C}_1 + \frac{\bar{C}_3}{\gamma} \right) - \frac{a^2\sigma Y}{\gamma} - \frac{a^2\chi\tau Y}{\gamma} - \tau\chi \left( \frac{3b\bar{Y}}{\bar{\gamma}} + \frac{3aY}{\gamma} \right) - 3\sigma \left( \frac{b\bar{Y}\bar{S}}{\bar{\gamma}} + \frac{aY}{\gamma} \right) - 3\chi\tau \left( \frac{2b\bar{Y}}{\bar{\gamma}} + \frac{bY}{\bar{\gamma}} + \frac{aY}{\gamma} \right) + 3\sigma \left( -\frac{2b\bar{S}\bar{Y}}{\bar{\gamma}} + \frac{b\bar{S}^2Y}{\bar{\gamma}} + \frac{aY}{\gamma} \right), \tag{A34}$$

$$C_{15} = 2\beta_- (\bar{C}_4\bar{S}\beta_+ + C_4\beta_-) + \bar{S}^2\beta_+^2 \left( \bar{C}_2 + \frac{3\bar{C}_3\beta_-}{\gamma} \right) + \frac{9\beta_-\alpha}{\gamma} (C_4 + \bar{C}_4) - \frac{3ab^2\bar{S}\beta_+\beta_-^2}{2\gamma} + 2\beta_-^2Y + \chi Y \left( \bar{C}_2 + \frac{3\bar{C}_3\beta_-}{\gamma} \right) - \frac{9\sigma\beta_-\bar{Y}}{\gamma} - \frac{27\beta_-\tau\chi Y}{\gamma} + \frac{9\bar{S}\beta_-^2Y}{4\gamma} - \frac{9\bar{S}\beta_-^3Y}{\gamma} + \frac{9\bar{S}\beta_-^2\beta_+Y}{\gamma} - \frac{3\beta_-^2}{\gamma} (\bar{S}C_4\beta_+ + C_4\beta_-) - \bar{S}^2\beta_+Y\beta_- \left( \bar{C}_2 + \frac{\bar{C}_3}{\gamma} \right) + \frac{9\beta_-^3}{\gamma}, \tag{A35}$$

$$\begin{aligned}
C_{16} = & 2c_1\bar{S}\beta_+(\bar{C}_4\bar{S}\beta_+ + C_4\beta_-) + c_1\beta_-^2 \left( C_2 - \frac{3C_3\beta_+}{\gamma} \right) + \frac{3\sigma\bar{S}c_1\beta_+}{\gamma} (\bar{S} - 2) \\
& (C_4 + \bar{C}_4) - \frac{9\bar{S}\beta_+^2\beta_-}{4\gamma} + \frac{27\chi\tau\beta_+}{2\gamma} (C_4 + \bar{C}_4) - \frac{9\bar{S}\sigma\beta_+\bar{Y}}{2\gamma} + \frac{9\chi\tau\bar{Y}}{2\gamma} + Y \\
& (C_4 + \bar{C}_4) + 2\bar{S}\beta_+\beta_-Y + \frac{9\beta_+\tau\chi}{2\gamma} (2\bar{Y} + Y) + \frac{9\sigma\beta_+\bar{S}}{2\gamma} (2\bar{Y} - \bar{S}Y) - \frac{9\bar{S}\beta_+^2\bar{Y}}{4\gamma} \\
& + \frac{81\bar{S}^2\beta_+^2\bar{Y}}{4\gamma} + \frac{63\bar{S}\beta_+^2\bar{Y}}{4\gamma} + \frac{18\bar{S}\beta_+\beta_-Y}{\gamma},
\end{aligned} \tag{A36}$$

$$C_{17} = b \left( \mathbf{LF}_8 + \mathbf{LF}_1 + \mathbf{LF}_7 + \frac{\mathbf{LF}_6 C_8}{\gamma} \right) + Sa\mathbf{LF}_8 A', \tag{A37}$$

$$C_{18} = b \left[ \frac{\mathbf{LF}_2}{2} + \mathbf{LF}_4 \bar{C}_9 + \mathbf{LF}_5 \bar{C}_9 + \mathbf{LF}_6 \left( \frac{4\bar{C}_{10}}{\gamma} - \frac{3\beta_+}{2\gamma} \right) \right], \tag{A38}$$

$$C_{19} = b \left( \frac{\mathbf{LF}_3}{3} + \mathbf{LF}_4 \bar{C}_{10} + \mathbf{LF}_5 \bar{C}_{10} - \frac{5\mathbf{LF}_6 \bar{C}_{10} \beta_+}{\gamma} \right). \tag{A39}$$

## Appendix C

$$\bar{C}_1 = \frac{\beta_+ + S\beta_-}{2\bar{C}_5\beta_+}, \tag{A40}$$

$$\bar{C}_2 = \frac{\beta_-(2\beta_+ + S\beta_-)}{\bar{C}_5\beta_+}, \tag{A41}$$

$$\bar{C}_3 = \frac{3S}{6\bar{C}_5\beta_+} (6\alpha - 3\beta_-^2 - \bar{S}\beta_+\beta_-), \tag{A42}$$

$$\bar{C}_4 = \frac{1}{\bar{C}_5} \left( \bar{S}\beta_+ + 2\beta_- + \frac{\bar{C}_c Y (\chi - \beta_+^2)}{\beta_+} \right), \tag{A43}$$

$$\bar{C}_5 = 2\beta_- - \frac{\bar{S}}{\beta_+} - \frac{\sqrt{\chi\bar{\chi}}}{\beta_+}. \tag{A44}$$

$$\begin{aligned}
\bar{C}_6 = & \frac{1}{2}C_1 + \frac{3C_3S\beta_-}{6\gamma^2} + \frac{C_3}{2\gamma} + \frac{3C_1S\beta_-}{6\gamma} \\
& - \frac{1}{\beta_+} \left[ -\frac{1}{2}C_1S\beta_- + \frac{9\bar{\chi}\Gamma}{\gamma^2} + \frac{3C_3\sigma}{\gamma^2} - \frac{9\beta_+^2}{24\bar{\gamma}^2} - \frac{3C_3S\beta_-\beta_+^2}{2\gamma} \right. \\
& \left. + \frac{3c_1\sigma}{\gamma} + \frac{3\beta_+}{4\gamma} - \frac{C_3S\beta_-}{2\gamma} + \frac{3c_1S\beta_-\beta_+}{2\gamma} - 3\bar{\chi}\tau \left( \frac{C_3}{\gamma^2} + \frac{C_1}{\gamma} \right) \right],
\end{aligned} \tag{A45}$$

$$\begin{aligned} \bar{C}_7 = & \left[ -2 \left\{ (\beta_+ + S\beta_-) \left( C_1 + \frac{C_3}{\gamma} \right) \right\} + \frac{1}{2} \left( C_2 - \frac{3\bar{C}_3\beta_+}{\gamma} \right) + (15C_3\beta_+ + 4C_2\bar{\gamma} \right. \\ & \left. + 3C_1\bar{\gamma}\beta_+) \frac{3S\beta_-}{6\bar{\gamma}^2} \right] - \frac{1}{\beta_+} \left[ 2S\beta_+\beta_- \left( C_1 + \frac{C_3}{\gamma} \right) - 3 \left( \frac{\alpha + c_1\beta_+\beta_-}{\bar{\gamma}^2} \right) (15\bar{C}_3\beta_- \right. \\ & \left. - 4\bar{C}_2\bar{\gamma} + 3\bar{\gamma}\bar{C}_1\beta_-) - \bar{c}_1S\beta_+ \left( C_2 + \frac{3C_3\beta_-}{\gamma} \right) - \frac{135\Gamma S^2\beta_+}{\bar{\gamma}^2} + \frac{45S^2\beta_+^3}{8\bar{\gamma}^2} + \frac{\beta_+^2}{4\bar{\gamma}} \right], \end{aligned} \tag{A46}$$

$$\begin{aligned} \bar{C}_8 = & -3c_1(\beta_+ + S\beta_-) \left( C_2 + \frac{3C_3\beta_-}{\gamma} \right) + 15c_1^2S\beta_- \left( \frac{3C_3\beta_+^2}{\bar{\gamma}^2} - \frac{C_2\beta_+}{\bar{\gamma}} \right) - \frac{1}{\beta_+} \\ & \left[ \frac{45c_1\beta_+ + (3C_3\beta_- - C_2\bar{\gamma})(2\alpha + S\beta_-\beta_+)}{\bar{\gamma}^2} + 3c_1S\beta_+\beta_- \left( C_2 - \frac{3C_3\beta_+}{\gamma} \right) + \frac{405\Gamma\chi\beta_+^2}{\bar{\gamma}^2} \right. \\ & \left. - \frac{135c_1S^2\beta_+^4}{8\bar{\gamma}^2} - \frac{27c_1\beta_+^3}{\bar{\gamma}} \right], \end{aligned} \tag{A47}$$

$$\bar{C}_9 = -\frac{4\bar{C}_8 - 3\bar{C}_7\beta_+}{9\beta_+^2}, \tag{A48}$$

$$\bar{C}_{10} = \frac{2\bar{C}_8}{3\beta_+}, \tag{A49}$$

$$\begin{aligned} \bar{C}_{11} = & c_1b(C_4 + \bar{C}_4) - 2(bS\beta_- + a\beta_+) \left( \bar{C}_1 + \frac{\bar{C}_3}{\gamma} \right) + \left( \frac{b}{\bar{Y}} + \frac{3a}{2Y} \right) (\bar{C}_4\beta_+ + C_4\beta_-S) \\ & - \frac{bS\bar{Y}}{2} + \frac{b\beta_+\bar{Y}}{6\bar{\gamma}} + \frac{a\beta_-YS}{2\gamma} + \frac{a\beta_+\bar{Y}}{2\gamma} + \frac{aS\beta_-Y}{\gamma}, \end{aligned} \tag{A50}$$

$$\begin{aligned} \bar{C}_{12} = & 2\beta_+(C_4 + \bar{C}_4) - 2(\bar{C}_4\beta_+ + C_4S\beta_-) - \beta_-S \left( C_2 - \frac{3C_3\beta_+}{\gamma} \right) - 2\beta_+\bar{Y} - \frac{3\beta_+^2\bar{Y}}{2\bar{\gamma}} \\ & - \frac{\beta_+}{2\bar{\gamma}} (\bar{C}_4\beta_+ + C_4S\beta_-), \end{aligned} \tag{A51}$$

$$\begin{aligned} \bar{C}_{13} = & (C_4 + \bar{C}_4) - (C_4S\beta_- + \bar{C}_4\beta_+) - 2\beta_+ \left( \bar{C}_2 + \frac{3\bar{C}_3\beta_-}{\gamma} \right) + \frac{3\beta_-}{4\gamma} (\beta_+\bar{Y} + 2S\beta_-Y) \\ & + \frac{9\beta_-}{4\gamma} (\bar{C}_4\beta_+ + C_4S\beta_-) + \beta_- (C_4 + \bar{C}_4)S\bar{Y} - (\beta_+ + S\beta_-) - \bar{Y}(\bar{C}_4\beta_+ + C_4S\beta_-) \\ & + \frac{3S\bar{Y}\beta_-^2}{4\gamma}, \end{aligned} \tag{A52}$$

$$\begin{aligned}
 \bar{C}_{14} = & -c_1b(\bar{C}_4\beta_+ + C_4S\beta_-) + (b\beta_-^2S^2 + a\beta_+^2) \left( \bar{C}_1 + \frac{\bar{C}_3}{\gamma} \right) + \frac{3a\beta_-YS^2}{\gamma} - \frac{3b\sigma\bar{Y}}{\gamma} \\
 & 3\sigma(\bar{C}_4 + C_4) \left[ \frac{b}{\bar{\gamma}} + \frac{S^2a}{\gamma} - \frac{2Sa}{\gamma} \right] - \frac{3\beta_+\beta_-S}{2} \left( \frac{b}{\bar{\gamma}} - \frac{a}{\gamma} \right) + \frac{3a\beta_-^2YS^2}{\gamma} + 3b\beta_+^2S^2 \\
 & \left( \frac{\bar{Y}}{\bar{\gamma}} + \frac{1}{\gamma} \right) - 3\tau\chi(C_4 + \bar{C}_4) \left( \frac{b}{\bar{\gamma}} + \frac{a}{\gamma} \right) + \frac{bS\beta_+\bar{Y}}{2} + b \left( C_1 + \frac{C_3}{\bar{\gamma}} \right) - \frac{3b\tau\chi\bar{Y}}{\bar{\gamma}} \\
 & - 3\tau\chi \left( \frac{b\bar{Y}}{\bar{\gamma}} + \frac{a\bar{Y}}{\gamma} + \frac{2aY}{\gamma} \right) + 3\sigma \left( \frac{b}{\bar{\gamma}} + \frac{aS^2}{\gamma} - \frac{2aSY}{\gamma} \right) - 3\tau\sqrt{\chi\bar{\chi}}S \left( \frac{\bar{Y}}{\bar{\gamma}} + \frac{Y}{\gamma} \right) \\
 & + 3 \left( \frac{b\bar{Y}}{\bar{\gamma}} + \frac{aSY}{\gamma} \right) + \frac{3}{2}S \left[ \beta_+\bar{Y} \left( \frac{b}{\bar{\gamma}} + \frac{a}{\gamma} \right) - \frac{\beta_-Y}{\gamma} (Sa - b) \right] + \frac{3b\beta_+^2\bar{Y}}{2\bar{\gamma}} \\
 & + 15S\beta_+\bar{Y} \left( \frac{b}{\bar{\gamma}} + \frac{a}{\gamma} \right) + \frac{9b\beta_+\bar{Y}}{\bar{\gamma}} + \frac{3aS^2\beta_-Y}{\gamma} + (bc_1\beta_+ + 3c_1a\beta_+ + aS\beta_-) \\
 & \frac{1}{\gamma} (\beta_+ + S\beta_-) - bS^2\bar{Y}\beta_-^2 \left( C_1 + \frac{C_3}{\bar{\gamma}} \right) + 3c_1S^2\beta_+\bar{Y}\beta_- \left( \frac{b}{\bar{\gamma}} + \frac{a}{\gamma} \right),
 \end{aligned} \tag{A53}$$

$$\begin{aligned}
 \bar{C}_{15} = & 2\beta_+(\bar{C}_4\beta_+ + C_4S\beta_-) + S\beta_-^2 \left( C_2 - \frac{3C_3\beta_+}{\bar{\gamma}} \right) - \frac{9\beta_+\sigma}{\bar{Y}} + \frac{27\beta_+\chi\tau\bar{Y}}{\bar{\gamma}} + \frac{18\beta_+^2\bar{Y}}{2\bar{\gamma}} \\
 & (C_4 + \bar{C}_4) + \frac{3S\beta_+^2\beta_-}{2\bar{\gamma}} - \frac{9\beta_+\chi\tau}{\bar{\gamma}}(C_4 + \bar{C}_4) + 2\beta_+^2\bar{Y} + \chi - S\beta_-^2a^2b \left( C_2 - \frac{3C_3\beta_+}{\bar{\gamma}} \right) \\
 & \bar{Y} \left( C_2 - \frac{3C_3\beta_+}{\bar{\gamma}} \right) + \frac{3\sigma\beta_+\bar{Y}}{\bar{Y}} - \frac{9\beta_+^2\bar{Y}}{\bar{\gamma}}(1 + S) - \frac{9\beta_+}{2\bar{\gamma}} (\bar{C}_4\beta_+^2 + C_4S\beta_-) - \frac{27\beta_+^3\bar{Y}}{2\bar{\gamma}},
 \end{aligned} \tag{A54}$$

$$\begin{aligned}
 \bar{C}_{16} = & S\beta_-(\bar{C}_4\beta_+ + C_4S\beta_-) + c_1\beta_+^2 \left( \bar{C}_2 + \frac{3\bar{C}_3\beta_-}{\gamma} \right) + \frac{3c_1\sigma S}{\gamma}(S - 2)(C_4 + \bar{C}_4) \\
 & + \frac{9c_1S\beta_+\beta_-^2}{2\gamma} + \frac{9c_1S^2\chi\tau\beta_-}{\gamma}(C_4 + \bar{C}_4) + S^2\chi\bar{Y}(C_4 + \bar{C}_4) + 4S\beta_+\beta_-\bar{Y} \\
 & + \frac{3b\sigma\beta_-YS}{2\gamma} - \frac{3S^2\chi\tau\beta_-Y}{2\gamma} - \frac{9\tau\chi S^2\beta_-}{2\gamma}(\bar{Y} + Y) + \frac{9S\sigma\beta_-}{2\gamma}(S\bar{Y} - 2Y) \\
 & + \frac{9\beta_-^2YS^2}{4\gamma} + \frac{18\beta_+\beta_-\bar{S}\bar{Y}}{\gamma} - \frac{63S\beta_-^2Y}{2\gamma}(1 + S) - S\bar{Y}\beta_-(\bar{C}_4\beta_+ + C_4S\beta_-) + \frac{9\beta_-\beta_+}{4\gamma} \\
 & (\bar{C}_4\beta_+ + S\beta_-C_4) - \frac{9S\beta_-^2}{2\gamma}(\bar{C}_4\beta_+ + S\beta_-C_4) + \frac{9\beta_+^2S\beta_-\bar{Y}}{2\gamma} + \frac{9S^2\beta_-^2Y}{4\gamma},
 \end{aligned} \tag{A55}$$

$$\bar{C}_{17} = a \left( \bar{\mathbf{L}}\mathbf{F}_1 + \bar{\mathbf{L}}\mathbf{F}_7 + \frac{\bar{\mathbf{L}}\mathbf{F}_6C_8}{\gamma} + \bar{\mathbf{L}}\mathbf{F}_8 \right) + \bar{S}b\bar{\mathbf{L}}\mathbf{F}_8B', \tag{A56}$$

$$\bar{C}_{18} = a \left[ \frac{\bar{\mathbf{L}}\mathbf{F}_2}{2} + \bar{\mathbf{L}}\mathbf{F}_4C_9 + \bar{\mathbf{L}}\mathbf{F}_5C_9 + \bar{\mathbf{L}}\mathbf{F}_6 \left( \frac{4C_{10}}{\gamma} + \frac{3\beta_-}{2\gamma} \right) \right], \tag{A57}$$

$$\bar{C}_{19} = a \left( \frac{\bar{\mathbf{L}}\mathbf{F}_3}{3} + \bar{\mathbf{L}}\mathbf{F}_4C_{10} + \bar{\mathbf{L}}\mathbf{F}_5C_{10} + \frac{5\bar{\mathbf{L}}\mathbf{F}_6C_{10}\beta_-}{\gamma} \right). \tag{A58}$$

## References

1. Xia, X.; Shen, H.T. Nonlinear interaction of ice cover with shallow water waves in channels. *J. Fluid Mech.* **2002**, *467*, 259–268. [[CrossRef](#)]
2. Milewski, P.A.; Vanden-Broeck, J.M.; Wang, Z. Hydroelastic solitary waves in deep water. *J. Fluid Mech.* **2011**, *679*, 628–640. [[CrossRef](#)]
3. Vanden-Broeck, J.M.; Părău, E.I. Two-dimensional generalized solitary waves and periodic waves under an ice sheet. *Philos. Trans. R. Soc. A Math. Phys. Eng. Sci.* **2011**, *369*, 2957–2972. [[CrossRef](#)] [[PubMed](#)]
4. Deike, L.; Bacri, J.C.; Falcon, E. Nonlinear waves on the surface of a fluid covered by an elastic sheet. *J. Fluid Mech.* **2013**, *733*, 394–413. [[CrossRef](#)]
5. Wang, P.; Lu, D.Q. Analytic approximation to nonlinear hydroelastic waves traveling in a thin elastic plate floating on a fluid. *Sci. China Phys. Mech. Astron.* **2013**, *56*, 2170–2177. [[CrossRef](#)]
6. Hedges, T.S. Combinations of waves and currents: An introduction. *Proc. Inst. Civ. Eng.* **1987**, *82*, 567–585. [[CrossRef](#)]
7. Schulkes, R.M.S.M.; Hosking, R.J.; Sneyd, A.D. Waves due to a steadily moving source on a floating ice plate. part 2. *J. Fluid Mech.* **1987**, *180*, 297–318. [[CrossRef](#)]
8. Bhattacharjee, J.; Sahoo, T. Interaction of current and flexural gravity waves. *Ocean Eng.* **2007**, *34*, 1505–1515. [[CrossRef](#)]
9. Bhattacharjee, J.; Sahoo, T. Flexural gravity wave generation by initial disturbances in the presence of current. *J. Mar. Sci. Technol.* **2008**, *13*, 138–146. [[CrossRef](#)]
10. Mohanty, S.K.; Mondal, R.; Sahoo, T. Time dependent flexural gravity waves in the presence of current. *J. Fluids Struct.* **2014**, *45*, 28–49. [[CrossRef](#)]
11. Lu, D.Q.; Yeung, R.W. Hydroelastic waves generated by point loads in a current. *Int. J. Offshore Polar Eng.* **2015**, *25*, 8–12.
12. Fenton, J.D.; Rienecker, M.M. A fourier method for solving nonlinear water-wave problems: Application to solitary-wave interactions. *J. Fluid Mech.* **1982**, *118*, 411–443. [[CrossRef](#)]
13. Lin, P. A numerical study of solitary wave interaction with rectangular obstacles. *Coast. Eng.* **2004**, *51*, 35–51. [[CrossRef](#)]
14. Khan, U.; Ellahi, R.; Khan, R.; Mohyud-Din, S.T. Extracting new solitary wave solutions of benney-luke equation and phi-4 equation of fractional order by using ( $g'/g$ )-expansion method. *Opt. Quantum Electron.* **2017**, *49*, 362. [[CrossRef](#)]
15. Abdel-Gawad, H.; Tantawy, M. Mixed-type soliton propagations in two-layer-liquid (or in an elastic) medium with dispersive waveguides. *J. Mol. Liq.* **2017**, *241*, 870–874. [[CrossRef](#)]
16. Gardner, C.S.; Greene, J.M.; Kruskal, M.D.; Miura, R.M. Method for solving the Korteweg-de Vries equation. *Phys. Rev. Lett.* **1967**, *19*, 1095–1097. [[CrossRef](#)]
17. Su, C.H.; Mirie, R.M. On head-on collisions between two solitary waves. *J. Fluid Mech.* **1980**, *98*, 509–525. [[CrossRef](#)]
18. Mirie, R.M.; Su, C.H. Collisions between two solitary waves. part 2. A numerical study. *J. Fluid Mech.* **1982**, *115*, 475–492. [[CrossRef](#)]
19. Dai, S.Q. Solitary waves at the interface of a two-layer fluid. *Appl. Math. Mech.* **1982**, *3*, 777–788.
20. Mirie, R.M.; Su, C.H. Internal solitary waves and their head-on collision. i. *J. Fluid Mech.* **1984**, *147*, 213–231. [[CrossRef](#)]
21. Mirie, R.M.; Su, C.H. Internal solitary waves and their head-on collision. ii. *Phys. Fluids (1958–1988)* **1986**, *29*, 31–37. [[CrossRef](#)]
22. Ozden, A.E.; Demiray, H. Re-visiting the head-on collision problem between two solitary waves in shallow water. *Int. J. Non-Linear Mech.* **2015**, *69*, 66–70. [[CrossRef](#)]
23. Marin, M.; Öchsner, A. The effect of a dipolar structure on the hölder stability in Green–Naghdi thermoelasticity. *Contin. Mech. Thermodynam.* **2017**, *29*, 1365–1374. [[CrossRef](#)]
24. Zhu, Y.; Dai, S.Q. On head-on collision between two gKdV solitary waves in a stratified fluid. *Acta Mech. Sin.* **1991**, *7*, 300–308.
25. Zhu, Y. Head-on collision between two mKdV solitary waves in a two-layer fluid system. *Appl. Math. Mech.* **1992**, *13*, 407–417.

26. Huang, G.; Lou, S.; Xu, Z. Head-on collision between two solitary waves in a Rayleigh-Bénard convecting fluid. *Phys. Rev. E* **1993**, *47*, R3830. [[CrossRef](#)]
27. Dai, H.H.; Dai, S.Q.; Huo, Y. Head-on collision between two solitary waves in a compressible Mooney-Rivlin elastic rod. *Wave Motion* **2000**, *32*, 93–111. [[CrossRef](#)]
28. Bhatti, M.M.; Lu, D.Q. Head-on collision between two hydroelastic solitary waves with Plotnikov-Toland's plate model. *Theor. Appl. Mech. Lett.* **2018**, *8*, 384–392. [[CrossRef](#)]
29. Bhatti, M.M.; Lu, D.Q. Head-on collision between two hydroelastic solitary waves in shallow water. *Qual. Theory Dynam. Syst.* **2018**, *17*, 103–122. [[CrossRef](#)]



© 2019 by the authors. Licensee MDPI, Basel, Switzerland. This article is an open access article distributed under the terms and conditions of the Creative Commons Attribution (CC BY) license (<http://creativecommons.org/licenses/by/4.0/>).